

Thermal Stability of F-Rich Phlogopite and K-Richterite During Partial Melting of Metasomatized Mantle Peridotite With Implications for Deep Earth Volatile Cycles

Steenstra, E. S.; Klaver, M.; Berndt, J.; Flemetakis, S.; Rohrbach, A.; Klemme, S.

DOI

[10.1029/2023JB028202](https://doi.org/10.1029/2023JB028202)

Publication date

2024

Document Version

Final published version

Published in

Journal of Geophysical Research: Solid Earth

Citation (APA)

Steenstra, E. S., Klaver, M., Berndt, J., Flemetakis, S., Rohrbach, A., & Klemme, S. (2024). Thermal Stability of F-Rich Phlogopite and K-Richterite During Partial Melting of Metasomatized Mantle Peridotite With Implications for Deep Earth Volatile Cycles. *Journal of Geophysical Research: Solid Earth*, 129(3), Article e2023JB028202. <https://doi.org/10.1029/2023JB028202>

Important note

To cite this publication, please use the final published version (if applicable).
Please check the document version above.

Copyright

Other than for strictly personal use, it is not permitted to download, forward or distribute the text or part of it, without the consent of the author(s) and/or copyright holder(s), unless the work is under an open content license such as Creative Commons.

Takedown policy

Please contact us and provide details if you believe this document breaches copyrights.
We will remove access to the work immediately and investigate your claim.

JGR Solid Earth

RESEARCH ARTICLE

10.1029/2023JB028202

Key Points:

- Partial melting experiments on metasomatized peridotite were performed to assess the thermal stability of F-bearing phlogopite and K-richterite
- The thermal stability of phlogopite containing several wt.% F exceeds continental and oceanic geotherms within the upper 150 km
- F-rich phlogopite would be stable in virtually all continental lithosphere, thereby acting as a major long-term sink for F and/or H

Supporting Information:

Supporting Information may be found in the online version of this article.

Correspondence to:

E. S. Steenstra,
e.s.steenstra@tudelft.nl

Citation:

Steenstra, E. S., Klaver, M., Berndt, J., Flemetakis, S., Rohrbach, A., & Klemme, S. (2024). Thermal stability of F-rich phlogopite and K-richterite during partial melting of metasomatized mantle peridotite with implications for deep Earth volatile cycles. *Journal of Geophysical Research: Solid Earth*, 129, e2023JB028202. <https://doi.org/10.1029/2023JB028202>

Received 3 NOV 2023
Accepted 19 FEB 2024


Author Contributions:

Conceptualization: J. Berndt, S. Klemme
Data curation: E. S. Steenstra
Formal analysis: E. S. Steenstra, M. Klaver, J. Berndt, S. Flemetakis
Funding acquisition: E. S. Steenstra, J. Berndt, S. Klemme
Investigation: E. S. Steenstra, S. Flemetakis, S. Klemme
Methodology: E. S. Steenstra, J. Berndt, S. Flemetakis, A. Rohrbach, S. Klemme
Resources: J. Berndt, S. Klemme
Supervision: J. Berndt, S. Klemme

© 2024. The Authors.

This is an open access article under the terms of the [Creative Commons Attribution License](https://creativecommons.org/licenses/by/4.0/), which permits use, distribution and reproduction in any medium, provided the original work is properly cited.

Thermal Stability of F-Rich Phlogopite and K-Richterite During Partial Melting of Metasomatized Mantle Peridotite With Implications for Deep Earth Volatile Cycles

E. S. Steenstra^{1,2} , M. Klaver¹, J. Berndt¹, S. Flemetakis^{1,3}, A. Rohrbach¹, and S. Klemme¹

¹Institute of Mineralogy, University of Münster, Münster, Germany, ²Faculty of Aerospace Engineering, Delft University of Technology, Delft, The Netherlands, ³Institute of Geochemistry and Petrology, ETH Zürich, Zürich, Switzerland

Abstract Phlogopite and K-richterite constitute important carrier phases for H and F in Earth's lithosphere and mantle. The relative importance depends on their stabilities at high pressure and temperature, which in turn depends on bulk composition. Most previous experimental studies focused on the thermal stability of phlogopite and K-richterite were conducted using simplified chemical compositions. Here, partial melting experiments on metasomatized and carbonated, OH ± F-bearing near-natural peridotite were performed at high pressures (2 and 5 GPa) and temperatures (1,100–1,350°C) to assess the thermal stability of F-free versus F-bearing phlogopite and K-richterite. Experimental results demonstrate that the thermal stability of F-bearing phlogopite is increased by >55°C/wt.% F, relative to F-free phlogopite, whereas K-richterite is absent in all experiments with significant degrees of melting (>2%). The thermal stability of phlogopite containing several wt.% F exceeds continental and oceanic geotherms within the upper 150 km. Fluorine-rich phlogopite would therefore be stable in virtually all of the continental lithosphere, only to be decomposed during large, regional melting events such as continental break-up, thereby acting as a major long-term sink for F and/or H. This could even be the case for the oceanic asthenosphere, depending on the oceanic geotherm of the area of interest.

Plain Language Summary Phlogopite and K-richterite are important minerals for the fluorine and hydrogen cycles of the Earth's interior. The effects of fluorine on the thermal stability of phlogopite and K-richterite was studied using a suite of high pressure, high temperature experiments, mimicking partial melting in Earth's upper mantle and lower crust. The experimental results show that F dramatically enhances the stability of phlogopite, implying phlogopite can retain F and H up to greater depths in the Earth than previously assumed. Fluorine does not significantly affect the thermal stability of K-richterite. Given that F is more compatible in phlogopite compared to H, our results show that phlogopite becomes increasingly more stable through time as F is preferentially incorporated over OH during fluid alteration at high temperatures. Fluorine-rich phlogopite may only be decomposed during large, regional melting events, such as continental break-up, thereby acting as a long-term carrier of F and to a lesser extent OH in the Earth's lower crust and/or upper mantle.

1. Introduction

Fluorine is likely the most abundant halogen in the terrestrial mantle (Klemme & Stalder, 2018; McDonough & Sun, 1995). Subduction is an efficient means of transport of F-rich surface-altered material into the upper mantle (e.g., Flemetakis et al., 2022), but the relative proportion of F returned to the surface through volcanism versus F transported into the deep Earth remains debated (e.g., Straub and Layne (2003), Grützner et al. (2017), Bekaert et al. (2021) and references therein). Although F is not efficiently mobilized from the subducting slab during dehydration, relative to heavier halogens, F is incompatible during partial melting of eclogite-facies sediments and altered oceanic crust (e.g., Beyer et al., 2016; Straub & Layne, 2003; Van den Bleeken & Koga, 2015). As such, slab-derived melts can enrich mantle wedge peridotite in F where it can be incorporated in metasomatic OH-bearing minerals such as K-richterite and phlogopite (e.g., Gervasoni et al., 2017; Hecker et al., 2020).

Phlogopite, apatite and K-richterite are commonly found in upper mantle samples from the metasomatized continental lithosphere (Dawson & Smith, 1977; Exley & Smith, 1982; Fumagalli & Klemme, 2015; Gregoire et al., 2002; Konzett et al., 2012) and can contain several wt.% of F (Foley et al., 1986b; Edgar et al., 1991; Klemme & Stalder, 2018; Hecker et al., 2020; Figure S1 in Supporting Information S1). Phlogopite in peridotite xenoliths can contain up to as much as 8 wt.% F (Liu et al., 2011; Figure S1 in Supporting Information S1). A median content of 0.34 wt.% F was recently proposed for phlogopite derived from mantle

Validation: M. Klaver, J. Berndt, S. Flemetakis
Visualization: M. Klaver, J. Berndt, S. Klemme
Writing – original draft: E. S. Steenstra, M. Klaver
Writing – review & editing: M. Klaver, J. Berndt, S. Flemetakis, S. Klemme

xenoliths and a peridotite massif in Europe and Africa (Hecker et al., 2020), comparable with the median obtained by incorporation of larger peridotitic phlogopite data sets (0.39 wt.%; Figure S1 in Supporting Information S1). Phlogopite phenocrysts present in lamproites, kamafugites and lamprophyres are also F-rich and contain on average 2.18, 3.50, and 1.7 wt.% F, respectively (Edgar et al., 1996). On the other hand, apatite is deemed to be negligible in terms of its role as a F carrier in the mantle (Konzett & Frost, 2009; Konzett et al., 2012) and hydroxyl-apatite has shown to be stable only along cold continental geotherms (i.e., $<40 \text{ mW m}^{-2}$; Konzett & Frost, 2009). Phlogopite and to a lesser extent K-richterite, could act as important hosts for H_2O , F and other volatiles, depending on their thermal stability, even when present in low modal abundances.

Elevated F contents potentially increase the stability of phlogopite and K-richterite during partial melting (e.g., Condamine & Médard, 2014; Foley, 1991; Jaques et al., 1984; Petersen et al., 1982; Peterson et al., 1991; Tareen et al., 1995, 1998; Yoder & Eugster, 1954). Although Foley et al. (1986a) and Vukadinovic and Edgar (1993) concluded that F increases the compositional and thermal range of phlogopite stability, these experiments were conducted in “simple” chemical systems, that is, in the absence of Fe and Ti. In the $\text{KAlSiO}_4\text{-Mg}_2\text{SiO}_4\text{-SiO}_2$ system, Foley et al. (1986a) reported an increase in the thermal stability of phlogopite containing ~5 to 7.5 wt.% F of $\sim 300^\circ\text{C}$, relative to F-free, water-saturated systems. Experiments conducted on dehydration melting of metagreywackes also suggest an important, positive effect of F on the thermal stability of phlogopite (Dooley & Patiño Douce, 1996). Condamine and Médard (2014) observed an increase of $\sim 100^\circ\text{C}$ of the thermal stability of phlogopite at 1 GPa in the presence of small amounts of F ($<0.79 \text{ wt.}\%$). Finally, Sun et al. (2022) conducted atomic level research on the effects of F on the structural stability of phlogopite using in situ high-temperature infrared-, Raman spectroscopy and X-ray powder diffraction. They proposed that O-H bonds and lattice modes are stiffer for F-rich phlogopite compared to F-poor phlogopite, resulting in greater stability of F-rich phlogopite at high temperatures. Previous data were thus mostly obtained in “simple” chemical systems, of which it is unclear if it can be applied to natural systems at all, or experiments were run in non-equilibrium, ambient pressure conditions (Sun et al., 2022). Here, we assess the effects of F on the thermal stability of phlogopite and K-richterite in complex compositions at P-T conditions directly relevant for partial melting of metasomatized mantle peridotite.

2. Materials and Methods

2.1. Experimental

High-pressure (P), high-temperature (T) experiments were performed to systematically study the potential effects of F on stability of K-richterite and phlogopite during partial melting of metasomatized continental lithosphere. Lower pressure (2 GPa) experiments were conducted in an end-loaded piston cylinder press and higher pressure ($\sim 5 \text{ GPa}$) experiments were conducted in a Walker-type multi-anvil apparatus, both at the University of Münster. Starting material compositions consisted of KLB-1 (the recommended composition of Davis et al., 2009) plus 5 wt.% of a K-richterite component and 5 wt.% of a phlogopite component (taken from the hydrous but F-free 6 GPa experiment Ma54 reported by Konzett, 1997). The F-free K-richterite and phlogopite from this particular experiment (Ma54) contained 2.17 and 4.37 wt.% H_2O , respectively (Konzett, 1997).

The KLB-1 composition is based on an off-cratonic, mildly-depleted (i.e., $\text{Al}_2\text{O}_3 = 3.51 \text{ wt.}\%$) lherzolite xenolith from Kilbourne Hole (USA; Davis et al., 2009 and references therein) and therefore considered to be most widely employed natural analog for moderately metasomatized mantle. The KLB-1 composition is slightly enriched in MgO and (mildly) depleted in SiO_2 , Al_2O_3 , CaO, Na_2O , and TiO_2 relative to current estimates of the primitive mantle (Palme & O'Neill, 2014; Table S1 in Supporting Information S1). The addition of a 5 wt.% component of phlogopite and 5 wt.% component of K-richterite to KLB-1 yields an overall bulk composition that is enriched in MgO, K_2O and Na_2O , and (mildly) depleted in Al_2O_3 , CaO, and FeO, relative to the primitive mantle (Table S1 in Supporting Information S1).

The KLB-1 and the K-richterite and phlogopite components were individually synthesized by thoroughly mixing the appropriate amounts of oxides, carbonates, and/or fluoride under ethanol for at least 30 min. The K-richterite and phlogopite components of 5 wt.% each were added separately. The volatile compositions of the K-richterite and phlogopite components were varied by considering three different OH:F abundances (OH:F = 100:0, OH:F = 50:50, and OH:F = 10:90 by weight) for both the phlogopite and K-richterite component. This corresponds to

an overall H₂O and F content of 0.32 and 0 wt.% in the OH:F = 100:0 bulk composition, 0.16 and 0.16 wt.% in the OH:F = 50:50 bulk composition and 0.03 and 0.29 wt.% in the OH:F = 10:90 bulk composition. Volatiles were added to the experiments by addition of the appropriate amounts of brucite Mg(OH)₂ and MgF₂. All experiments were performed using Au₈₀Pd₂₀ outer and/or graphite (inner) capsules. Graphite (inner) capsules were chosen to (a) minimize potential Fe loss from the starting composition, (b) to facilitate quantitative comparison of our new results with previous studies on Fe-bearing compositions (Foley et al., 2022; Konzett & Frost, 2009) and (c) to provide an upper limit for oxygen fugacity. However, the use of graphite capsules resulted in the presence of significant quantities of CO₂ in the silicate melt (<10 wt.%). It also imposed an oxygen fugacity lower than the CCO (carbon – carbon monoxide/carbon dioxide) buffer (Dasgupta et al., 2007; Frost & Wood, 1997). This could imply that the redox conditions of the experiments were slightly more reducing than estimated for the lithospheric upper mantle (FMQ –3 to +1; e.g., Ballhaus, 1993). Experiments in the piston cylinder press were conducted using talc-pyrex assemblies, with an inner boron-nitride container containing the three Au₈₀Pd₂₀ capsules (with inner graphite capsules) as well as crushable Al₂O₃ spacers. Piston cylinder experiments were performed with 2.1 mm O.D. Au₈₀Pd₂₀ outer capsules and 1.7 mm O.D., 0.7 mm I.D. graphite inner capsules with a length of 3–4 mm. In multi-anvil experiments AuPd outer capsules could not be used due to size limitations and only graphite capsules (1.95 mm O.D., 0.9 mm I.D., height of 1.5 mm) were used.

Experiments in the piston cylinder press could be conducted for three compositions at a given set of P-T conditions, whereas in the multi-anvil press only two samples could be run per experiment due to smaller assembly size and larger thermal gradients. However, runs ESS-223-1 and ESS-224-1 were performed using only one capsule in the piston cylinder press. Both capsules in the multi-anvil experiments were stacked to reduce thermal gradients and the top capsule was fitted and closed with a graphite 0.5 mm thick disc. Temperatures were in all cases monitored and controlled using Eurotherm 2604 controllers and type C (95%W/5%Re-74%W/26%Re, by weight) thermocouples. Pressure calibration for the piston cylinder talc-pyrex assembly is based on the MgCr₂O₄ + SiO₂ = MgSiO₃ + Cr₂O₃ reaction (Klemme & O'Neill, 1997), yielding an overall friction correction of 13%. Estimated pressure uncertainties for this set-up are approximately ~0.1 GPa (e.g., Flemetakis et al., 2022; van Kan Parker et al., 2011). The temperature gradient throughout the capsule for the latter experiments is estimated to be ~20°C, with a thermal gradient of ~10°C/mm with increasing distance from the hotspot (Sorbadere et al., 2013; Watson et al., 2002). Multi-anvil experiments were conducted using a 18/12 assembly, with MgO, Cr-doped octahedra consisting of a zirconia sleeve that surrounded a graphite furnace. The pressure calibration of this particular assembly at high temperature is based on the quartz-coesite (3 GPa, 1,100°C; Bose & Ganguly, 1995) and CaGeO₃ garnet to perovskite (6 GPa, 1,100°C, Susaki et al., 1985) transitions, which yields a pressure uncertainty of ~0.5 GPa (e.g., Dai & Karato, 2009; Fedortchouk et al., 2019). The thermal gradients for the latter assembly are estimated to be ~20°C in the central 3 mm of the assembly, where both samples are positioned (Knibbe et al., 2018; Van Westrenen et al., 2003). Run durations varied between 3 and 51 hr (Table 1). After the experiments were rapidly quenched, the charges were mounted in epoxy resin, finely polished using various grades of Al₂O₃ powder and carbon-coated for electron microprobe measurements.

2.2. Analytical

Experimental run products were measured with a JEOL JXA-8530F field emission electron probe microanalyser for major and minor element abundances at the University of Münster, Germany (Table S2 in Supporting Information S1). Minerals were measured using a defocused beam (1–2 μm) and beam currents of 15–20 nA. For the latter measurements an accelerating voltage of 15 kV was applied. For silicate melts, spot sizes of 10–20 μm (where possible) were used due to the highly heterogeneous textures of the silicate melts. Measurements were mostly conducted in raster grids or lines, depending on the available surface area of the measured phases, while avoiding measurement of areas close to the edge of phases and/or surrounding capsule materials. For all elements, except F, counting times of 10–30 s on peak and 5–15 s on each background were applied. Fluorine contents in silicates and minerals were measured using an accelerating voltage of 15 kV. The counting times were 120 s on the peak and 60 s on the background, using beam currents of 60 nA (see Steenstra et al., 2020). Fluorine detection limits were reduced by using high beam currents and longer counting times, while preventing any loss of F under the beam as demonstrated by C. Zhang et al. (2016). Fluorine background was measured on the high-wavelength side only because of the FeLa interference on the low side. Measured F contents of the minerals or silicate melts were corrected for the interference with Fe (C. Zhang et al., 2016). These corrections were done using calibration curves based on measurements of nominally F-free glasses or minerals with variable FeO concentrations. To

Table 1
Experimental Run Conditions

	Starting composition	T (°C)	P (GPa)	Time (hr)	Observed phases ^a	Modal proportions											D _F ^{Pl-melt}
						Ol	Opx	K-rt	Cpx	Phl	Spl	Grt	Melt	Residual	K _D ^{Mg-Fe}	Ol-melt	
ESS-166-1	OH:F = 100:0	1,100	2.0	48	Ol, Opx, K-rt, Cpx, Phl, Spl	51	23	10	9	7	<1	-	-	0.01	-	-	-
ESS-166-2	OH:F = 50:50	1,100	2.0	48	Ol, Opx, K-rt, Cpx, Phl, Spl	51	23	13	7	6	<1	-	-	0.02	-	-	-
ESS-166-3	OH:F = 10:90	1,100	2.0	48	Ol, Opx, K-rt, Cpx, Phl, Spl	51	23	14	6	6	<1	-	-	0.22	-	-	-
ESS-220-1	OH:F = 50:50	1,125	2.0	47	Ol, Opx, K-rt, Cpx, Phl, Spl	53	22	13	7	6	<1	-	-	0.06	-	-	-
ESS-220-2 ^b	OH:F = 10:90	1,125	2.0	47	Ol, Opx, K-rt, Cpx, Phl	50	24	14	6	6	-	-	-	0.0002	-	-	-
ESS-222-1	OH:F = 100:0	1,125	2.0	43	Ol, Opx, K-rt, Cpx, Phl, Spl	53	21	12	8	7	<1	-	-	0.07	-	-	-
ESS-221-1 ^c	OH:F = 50:50	1,150	2.0	48	Ol, Opx, K-rt, Cpx, Phl, melt	53	22	10	9	7	-	-	1	0.0023	0.40	0.76 (13)	1.30 (17)
ESS-221-2 ^d	OH:F = 10:90	1,150	2.0	48	Ol, Opx, K-rt, Cpx, Phl, melt	48	25	12	7	6	-	-	2	0.0004	0.43	0.87 (12)	1.70 (20)
ESS-224-1	OH:F = 100:0	1,150	2.0	27	Ol, Opx, K-rt, Cpx, Phl, Spl	53	23	3	14	8	<1	-	-	0.02	-	-	-
ESS-223-1	OH:F = 100:0	1,175	2.0	24	Ol, Opx, Cpx, Phl, melt	58	17	-	12	6	-	-	8	0.02	0.37	-	-
ESS-207-2	OH:F = 10:90	1,175	2.0	48	Ol, Opx, Cpx, Phl, melt	56	18	-	10	7	-	-	9	0.03	0.38	-	1.13 (33)
ESS-207-3	OH:F = 50:50	1,175	2.0	48	Ol, Opx, Cpx, Phl, melt	57	17	-	11	6	-	-	9	0.04	0.39	-	1.24 (30)
ESS-199-1	OH:F = 100:0	1,250	2.0	48	Ol, Opx, Cpx, melt	61	13	-	8	-	-	-	18	0.03	0.33	-	-
ESS-199-2	OH:F = 10:90	1,250	2.0	48	Ol, Opx, Cpx, Phl, melt	58	16	-	7	3	-	-	16	0.04	0.35	-	1.49 (15)
ESS-199-3	OH:F = 50:50	1,250	2.0	48	Ol, Opx, Cpx, Spl, melt	59	17	-	5	-	<1	-	19	0.07	0.33	-	-
ESS-206-1	OH:F = 10:90	1,350	2.0	51	Ol, Opx, melt	60	14	-	-	-	-	-	26	0.13	0.34	-	-
ESS-206-2	OH:F = 100:0	1,350	2.0	51	Ol, Opx, Cpx, melt	62	10	-	4	-	-	-	24	0.08	0.32	-	-
ESS-206-3	OH:F = 50:50	1,350	2.0	51	Ol, Opx, melt	59	13	-	-	-	-	-	28	0.12	0.34	-	-
ESS-MA-2-1	OH:F = 10:90	1,250	5.0	39.3	Ol, Opx, Cpx, Phl, Grt, melt	47	21	-	12	4	-	10	7	0.04	0.32	-	0.38 (25)
ESS-MA-2-2	OH:F = 100:0	1,250	5.0	39.3	Ol, Opx, Cpx, Grt, melt	49	18	-	10	-	-	9	13	0.005	0.33	-	-
ESS-MA-7-1	OH:F = 100:0	1,275	5.0	24.5	Ol, Opx ^a , Cpx, Grt, melt	52	13	-	5	-	-	11	19	0.01	0.33	-	-
ESS-MA-7-2	OH:F = 10:90	1,275	5.0	24.5	Ol, Opx ^a , Cpx ^a , Grt, melt	53	13	-	4	-	-	11	18	0.04	0.29	-	-
ESS-MA-4-1	OH:F = 100:0	1,325	5.0	29	Ol, Opx [*] , Cpx, Grt, melt [*]	53	14	-	6	-	-	10	17	0.06	-	-	-
ESS-MA-4-2	OH:F = 10:90	1,325	5.0	29	Ol, Opx [*] , Cpx, Grt, melt [*]	54	12	-	6	-	-	11	16	0.04	-	-	-
ESS-MA-6-1	OH:F = 100:0	1,350	5.0	3.17	Ol, Opx, Cpx, Grt, melt	50	18	-	6	-	-	14	12	0.008	0.35	-	-
ESS-MA-6-2	OH:F = 10:90	1,350	5.0	3.17	Ol, Opx, Cpx, Grt, melt	54	15	-	8	-	-	13	11	0.03	0.29	-	-

Note. All experimental starting compositions consisted of 90% KLB-1 + 5 wt.% K-rt + 5 wt.% Phl but with variable OH:F (see Table S1 in Supporting Information S1). The OH:F ratios of 100:0, 50:50, and 10:90 of the KLB-1 starting mixtures correspond to 0.32 wt.% H₂O and 0 wt.% F, 0.16 wt.% H₂O and 0.16 wt.% F, and 0.03 wt.% H₂O and 0.29 wt.% F, respectively. ^aOl-olivine, Opx-orthopyroxene, K-rt-K-richite, Cpx-clinopyroxene, Phl-phlogopite, Spl-spinel, Grt-garnet. ^bOpx, Cpx and/or melt of runs MA-4-1,2 and MA-7-1,2 were not readily observed in the cross section and their abundances were calculated from least square regressions. ^cThis run suffered approximately 0.9 wt.% FeO loss. ^dThis run suffered approximately 0.5 wt.% FeO loss. ^eThis run suffered approximately 2.4 wt.% FeO loss.

ensure data precision and accuracy, F was measured in reference glasses USNM Rhyolite VGA-568, NIST 610, USNM Makaopuhi A-99, USNM Juan da Fuca VG-2 and BCR2-G throughout the study, as in previous work (Flemetakis et al., 2020; Steenstra et al., 2020).

Mineral modes were obtained by performing least-square regressions based on seven components (SiO_2 , Al_2O_3 , MgO , CaO , FeO , Na_2O , and K_2O). For the measurements of the more challenging MA experiments, uncertainties on derived modal abundances were assessed by performing Monte Carlo simulations with 10,000 iterations per experimental run. Obtained modes were largely unaffected by consideration of the different subsets of components, demonstrating the robustness of the results.

3. Results

3.1. Run Products and Attainment of Equilibrium

Experimental samples were composed of silicate minerals ($\text{Ol} \pm \text{Opx} \pm \text{Cpx} \pm \text{K-rct} \pm \text{Phl} \pm \text{Grt} \pm \text{Spl}$) and quenched silicate melt, depending on pressure, temperature and composition (Table 1). Run products that contained melt generally showed clear segregation of the melt from the crystals to the hottest side of the experiments, (Figure 1). This is due to the inevitable presence of temperature gradients in the charge that promote thermally induced compaction of melt away from solid (Walter, 1998). A steady-state can be achieved despite this segregation, where the observed phase compositions reflect the average “equilibrium” conditions of the entire experimental capsule (Leshner & Walker, 1988; Walter, 1998). The efficient segregation of melt generally resulted in relatively large ($>15 \mu\text{m}$) pools of melt that contained fine-grained quench crystals at relatively low melt fractions (down to 1 to 2 modal % melt).

High pressure-temperature experiments were performed for durations ranging from three to 51 hr, depending on temperature and experimental assembly. The run times for piston cylinder experiments (>24 hr, but mostly >47 hr) are comparable or in some cases much longer than previous studies that focused on similar processes conducted in similar assemblies at comparable temperatures (e.g., Foley et al., 1986a; Hirose & Kawamoto, 1995; Sorbadere et al., 2018; Vukadinovic & Edgar, 1993; Y. Zhang et al., 2020). Run durations used for multi-anvil experiments were at least 3 hr, but mostly >20 hr Hirose and Kawamoto (1995) found that under hydrous conditions equilibrium was attained within 11.5 hr at 1,300°C and 1 GPa, respectively, for sample containers with an inner diameter of 4.7 mm. This is much larger than the inner diameter of the graphite capsules used in our multi-anvil experiments (~ 0.8 mm), suggesting that the experiments conducted for slightly over 3 hr at 1,350°C must have attained equilibrium as well (Table 1). Results from liquidus experiments performed by Presnall et al. (1978) show that appearance and disappearance of phases is much faster than homogenization of their phase compositions, that is, 2–4 hr for peridotite phases crystallized from a silicate melt at 1,400–1,600°C (Walter, 1998). Almost all of the reported experiments were conducted at much longer run durations, which should have resulted in equilibration. It should be noted that the high H_2O content of the melt also strongly promotes diffusion within the experiments, confirmed by near-identical mineral compositions for the different experiments (Table S2 in Supporting Information S1). The Fe-Mg K_D between olivine and melt varies between 0.29 and 0.43, which is generally within the estimated values for equilibrium experiments (see Figure 9a from Blundy et al., 2020; Roeder & Emslie, 1970; Table 1). Most values cluster around 0.32–0.35, and the anomalously higher values of 0.37–0.43 for the lowest P-T experiments could be a result of minor disequilibrium presumably due to the very low degree of melting. Finally, the minerals produced in our experiments did not show compositional zonation from core to rim.

In some of the multi-anvil experiments (MA4-1,2), melt was not observed although the presence of it is suggested by mass balance (Table 1). The melts of these experiments could therefore not be measured. This is most likely the result of relatively small melt fractions (<17 modal %) and concentration of the melt in a particular area not exposed in the mounted experimental run product (Walter, 1998). Finally, we were unable to locate Opx and/or Cpx in runs MA7-1,2, although including these as phases significantly improves least square regression results, suggesting they were present in the sample(s) but not in the cross-section considered (Table 1).

3.2. General Phase Relations and Melting Reactions

The first, low degree partial melts were observed at approximately 1,150°C (2 GPa) and 1,250°C (5 GPa), suggesting that the solidus temperatures for these compositions are slightly below these temperatures (Figures 2–4).

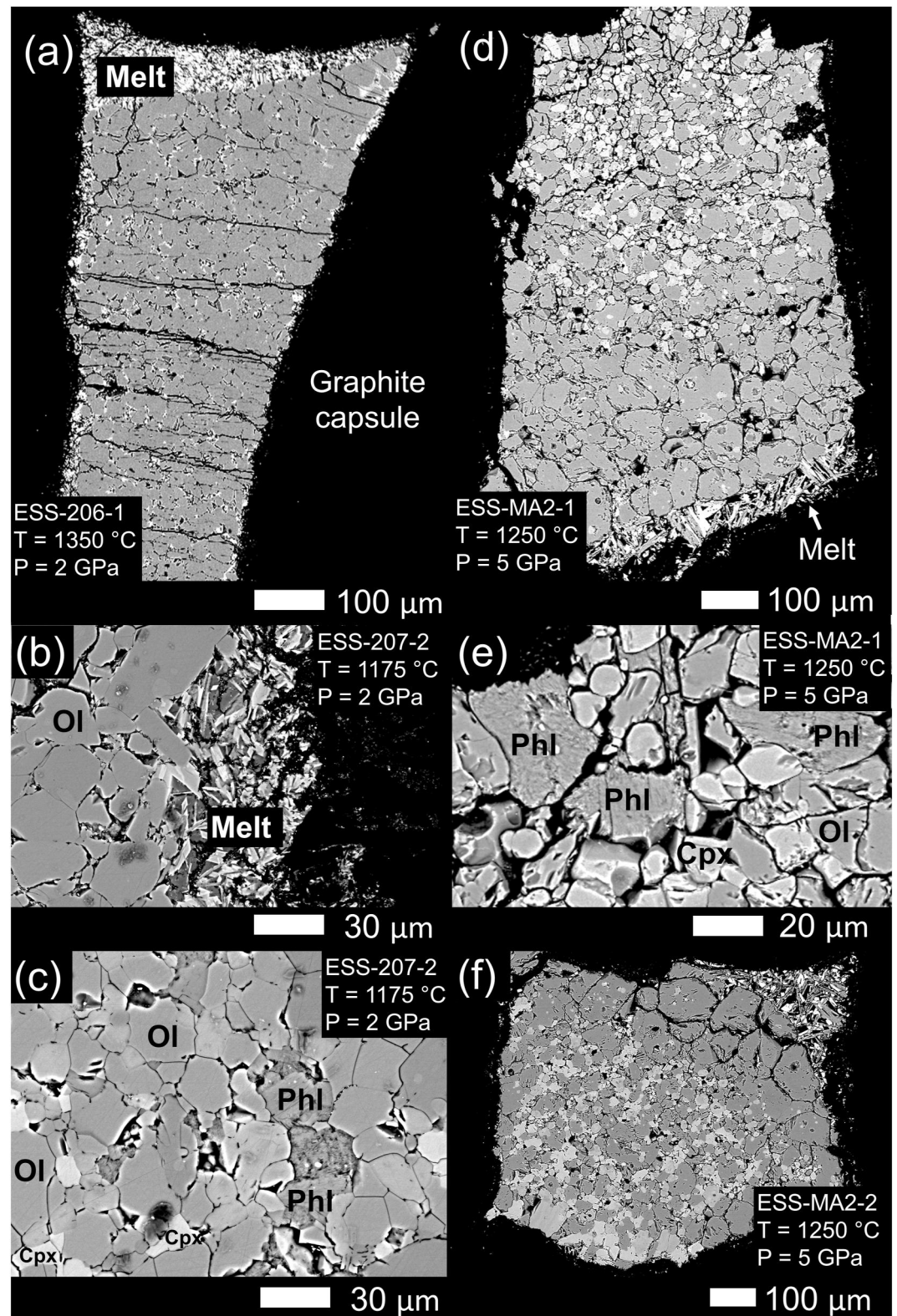


Figure 1. Backscattered electron-images depicting typical examples of experimental run products (a–c) Experimental charges obtained at 2 GPa. (d–f) Experimental run products synthesized at 5 GPa. In all experiments with melt present, the melt migrated to the hotspot region (see panels a, d, f).

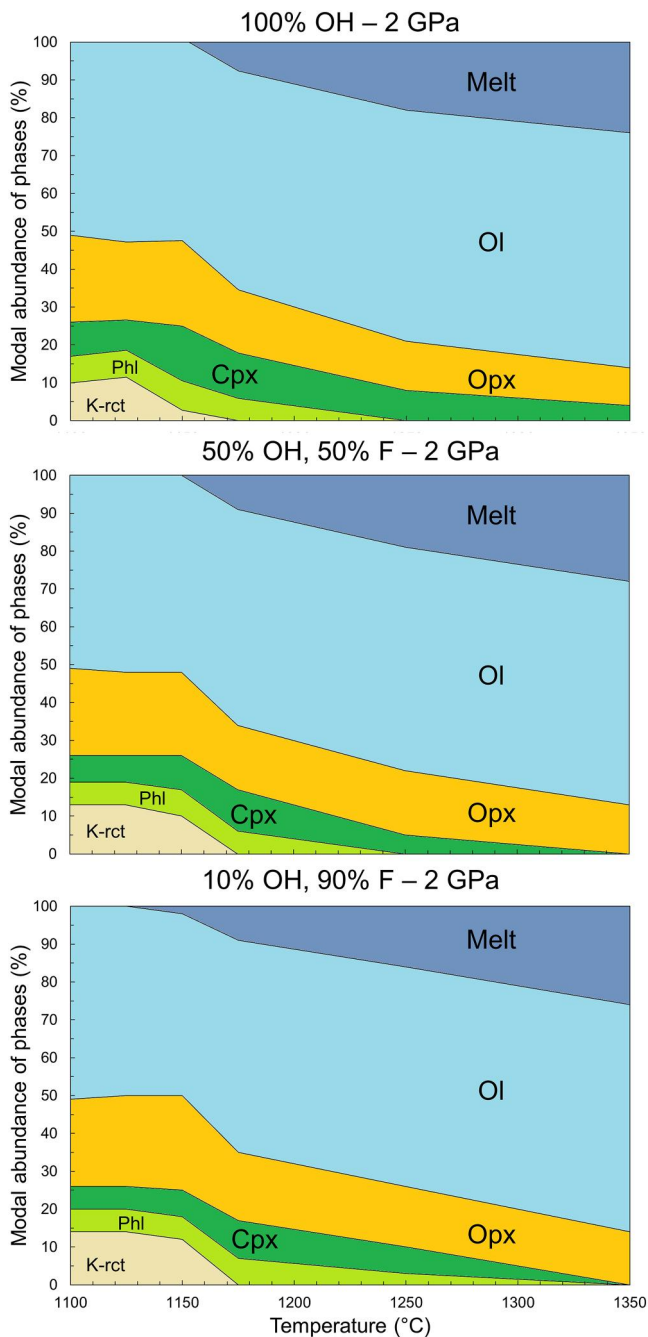


Figure 2. Calculated modal abundances of minerals and melt as a function of experimental peak temperatures at 2 GPa for the system 90 wt.% KLB-1 + 5 wt.% Phl (OH:F = 100:0) + 5 wt.% K-rt (OH:F = 100:0) (top panel), corresponding to a bulk H₂O and F content of 0.32 and 0 wt.%, 90 wt.% KLB-1 + 5 wt.% Phl (OH:F = 50:50) + 5 wt.% K-rt (OH:F = 50:50) (middle panel), corresponding to a bulk H₂O and F content of 0.16 and 0.16 wt.%, and 90 wt.% KLB-1 + 5 wt.% Phl (OH:F = 10:90) + 5 wt.% K-rt (OH:F = 10:90) (bottom panel), corresponding to a bulk H₂O and F content of 0.03 and 0.29 wt.%, respectively.

However, the apparent lack of a further increase in the degree of melting in the 5 GPa runs between 1,275 and 1,350°C is most readily explained by the termination of the initial decomposition of phlogopite, after which the remaining mineral assemblage remains stable up to much higher temperatures (Figures 3 and 4). This strongly suggests that phlogopite determines the solidus temperature of this system (Sudo & Tatsumi, 1990; Trønnes et al., 1988). Indeed, the solidus for dry fertile peridotite is ~1,600°C (Kawamoto, 2004; Walter, 2003 and references therein) at 5 GPa. No clear differences were observed in the amount of melt present for different bulk compositions (Table 1). The presence of abundant feathery and dendritic crystallite and felt-like masses, in conjunction with the apparent absence of spherule-sheet mixtures, suggests the experimental melts were undersaturated in water (Wang et al., 2020 and references therein). This agrees with the generally much lower added H₂O amounts (<0.33 wt.% H₂O) relative to the maximum water-storage capacity estimated for peridotite (<0.5 wt.%; Green et al., 2010).

The use of graphite inner capsules resulted in the presence of CO₂ in the melt, which could affect its solidus temperature (e.g., Pintér et al., 2021; Wylie, 1987) and therefore the stability of hydrous phases, including K-richterite (Foley et al., 2022, and references therein). Although the CO₂ contents could not be determined quantitatively due to the dendritic nature of the melts, the silicate melt CO₂ contents can be estimated. The results of Ghosh et al. (2014) for fertile and alkali-rich peridotitic compositions show that the CO₂ content of the melt strongly correlate with both SiO₂ and CaO (e.g., Pintér et al., 2021). Considering the melt compositions of this study (42.0–54.1 wt.% SiO₂, 5.2–9.9 wt.% CaO), in conjunction with the explored *P-T* conditions, suggests that silicate melt CO₂ contents are unlikely to exceed 10 wt.% (Ghosh et al., 2014). Finally, the use of graphite inner capsules and the corresponding potentially more reducing conditions, relative to redox states commonly inferred for the lithospheric mantle, could affect the thermal stabilities of the hydrous phases of interest.

K-richterite and spinel were found to be only stable at the lowest *P-T* experiments (<1,150°C), independent of bulk composition (Figures 2–4). At 5 GPa, K-richterite was not observed to be stable at a temperature down to 1,250°C. The absence of K-richterite in all experiments with significant amounts of melt present (>8 modal %) is consistent with the observations of Foley et al. (2022) that K-richterite is exhausted at only a few tens of °C above the solidus. At 5 GPa, and therefore in the presence of garnet, K-richterite is not stable, as it only re-appears after breakdown at pressures exceeding 6 GPa due to the reaction $\text{Phl} + \text{Cpx} + \text{Opx} = \text{K-rt} + \text{Grt} + \text{Ol} + \text{fluid}$ (Konzett & Ulmer, 1999). Olivine and orthopyroxene were observed (or their presence was suggested by mass balance) in all experiments (Table 1). Phlogopite was found to be stable up to 1,250°C at both 2 and 5 GPa, but only for the most F-rich bulk composition (Table 1).

3.3. Mineral and Melt Compositions

3.3.1. Melts

Table S2 in Supporting Information S1 and Figure 5 show the experimental melt compositions. The measured melt compositions obtained from experiments performed at 2 GPa plots in the basaltic andesite, basalt to basaltic trachyandesite field, whereas at 5 GPa, low-degree partial melts are significantly more Na₂O and K₂O-rich and can be classified as (phono)-tephrite or

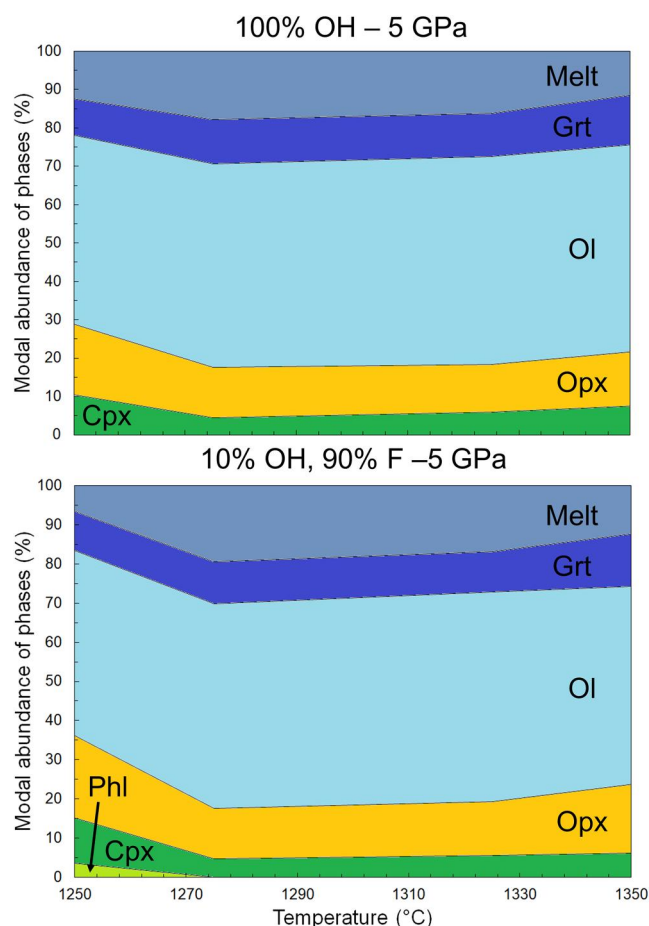


Figure 3. Modal abundances of minerals and melt as a function of experimental peak temperatures at 5 GPa for the system 90 wt.% KLB-1 + 5 wt.% Phl (OH:F = 100:0) + 5 wt.% K-rt (OH:F = 100:0) (top panel), and 90 wt.% KLB-1 + 5 wt.% Phl (OH:F = 10:90) + 5 wt.% K-rt (OH:F = 10:90) (bottom panel). See caption of Figure 2 for additional compositional details.

foidite (Figure 5). With increasing melt production, MgO, CaO, and FeO contents generally increase and/or remain constant, whereas Na₂O, Al₂O₃, and TiO₂ decrease, largely consistent with the observations of Walter (1998) for melting of garnet peridotite (Figure S2 in Supporting Information S1). However, the overall melt compositions of the experiments are very different compared to low degree melts of garnet peridotite at similar pressures. The melts reported here are, as expected, richer in K₂O and Na₂O and thus have much higher K₂O/CaO and K₂O/MgO (Figure S3 in Supporting Information S1). Melt K₂O/Al₂O₃ ranges between 0.08 and 1.40, with an overall increase from 2 to 5 GPa (Figure S4 in Supporting Information S1), which is due to the retention of Al₂O₃ from in the residua in the presence of garnet in the 5 GPa runs. The TiO₂ contents overlap or are slightly elevated compared to garnet peridotite melting (Walter, 1998).

3.3.2. Clinopyroxene, Orthopyroxene, Garnet

Clinopyroxene in the experiments is diopside, and is partly incongruent during the breakdown of K-richterite and phlogopite in the various experiments (Foley et al., 2022). Clinopyroxene, orthopyroxene and garnet compositions are all very similar to mineral compositions from a previous anhydrous melting studies on KLB-1 at comparable pressures (Takahashi, 1986). The only exception is the Al₂O₃ contents of both Cpx and Opx, a result of the much higher temperatures at which the experiments of Takahashi (1986) were conducted.

3.3.3. Phlogopite and K-Richterite

The compositions of K-richterite measured in this study compositionally overlap with the majority of the experimental data previously reported (Table S2, Figure S5 in Supporting Information S1; Foley et al., 2022; Konzett, 1997). Phlogopite shows most compositional variation in Mg, Si, Ti, and Al contents. The Ti and Al contents correlate positively, whereas Al and Ti contents decrease with Mg and Si concentrations (Table S2 in Supporting Information S1). In addition, the Fe and F contents of phlogopite at a given bulk composition are strongly correlated, reflecting the F-Fe avoidance rule, that is, an increase of F in phlogopite yields a decrease of Fe and vice-versa (Munoz, 1984; Figure S6 in Supporting Information S1). The derived phlog-

opite/silicate melt partition coefficients for F ($D_F^{(Phl-melt)}$, defined as the ratio between the weight concentration of F in phlogopite and silicate melt, respectively) range between 0.38 ± 0.25 to 1.70 ± 0.20 for all of the experiments considered, within the range of previously reported values (e.g., Edgar & Pizzolato, 1995; Flemetakis et al., 2021). The range is explained by variation in melt compositions and variable P-T conditions (Edgar & Pizzolato, 1995; Ezad & Foley, 2022). Fluorine is mildly incompatible in K-richterite, with $D_F^{(K-rt-melt)}$ values of 0.76 ± 0.13 to 0.87 ± 0.12 , consistent with previous experiments at 2 GPa and comparable temperatures (Edgar & Pizzolato, 1995).

3.3.4. Quantification of the Effects of F on K-Richterite and Phlogopite Thermal Stability

The new phase relations can be used to quantify the effects of F on the thermal stability of K-richterite and phlogopite. Our results show that the effect of F on K-richterite stability is negligible within the explored compositions and P-T conditions. It should be noted that our results disagree with earlier findings for K-richterite and/or pargasite (Foley, 1991; Holloway & Ford, 1975). This may be explained by several reasons. First, Foley (1991) reported that the thermal stabilities of the OH- and F-endmembers of K-richterite differ only by 100 degrees at 3.5 GPa and this effect is likely smaller at 2 GPa. However, the F content of fluoro-K-richterite from Foley (1991) is ~2.6 wt.% which is almost 3 times higher than the highest F content measured for K-richterite in this study (~0.9 wt.%, and usually less). It is therefore not surprising that no effects of F on the thermal stability of

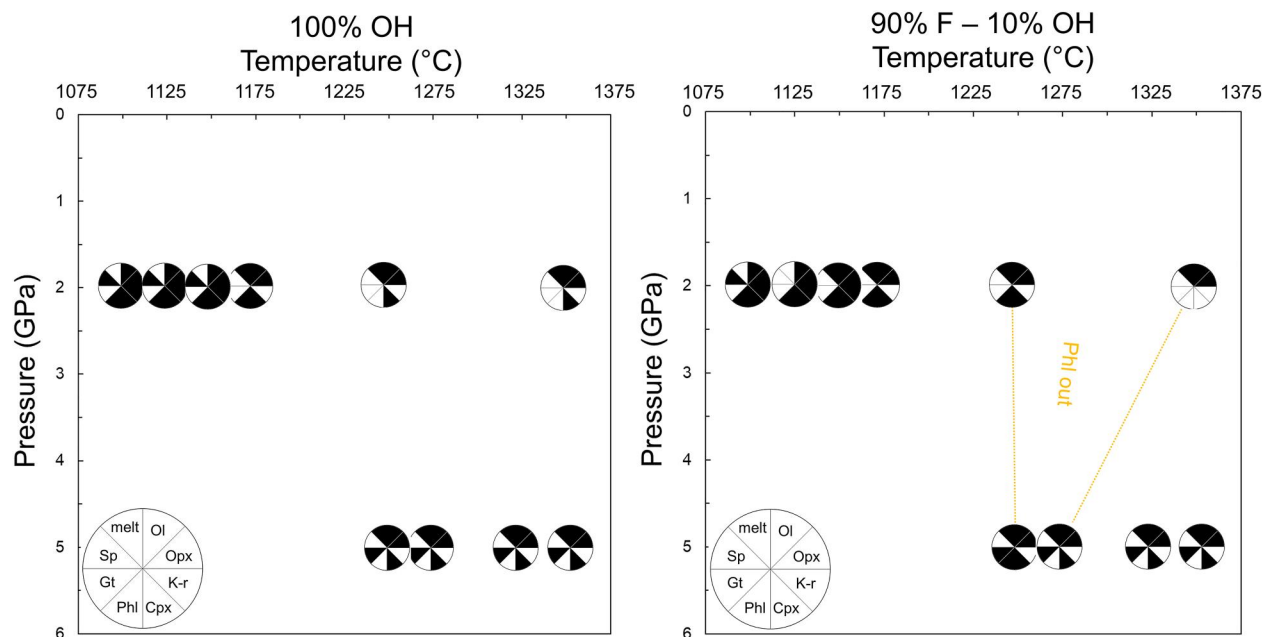


Figure 4. Phase relations at 2 and 5 GPa for the system 90 wt.% KLB-1 + 5 wt.% Phl (OH:F = 100:0) + 5 wt.% K-rt (OH:F = 100:0) (left panel) and the system 90 wt.% KLB-1 + 5 wt.% Phl (OH:F = 10:90) + 5 wt.% K-rt (OH:F = 10:90) (right panel). See caption of Figure 2 for additional details.

K-richterite were observed in this study. In addition, the fluoro-K-richterites reported by Foley (1991) were Fe-free, whereas the F-bearing K-richterite phases from this study contain 2.44 to 3.81 wt.% FeO. As an increase of FeO likely reduces the thermal stability of K-richterite (Frost, 2006), Fe-poor K-richterite is destabilized at lower *P-T* conditions. It has also been shown that the stability of pargasitic amphibole is affected by the bulk alkali content of the system under water-undersaturated conditions (Niida & Green, 1999; Wallace & Green, 1991). An increase in the glaucophane, richterite, edenite and Ti tschermakite components of amphibole yields higher thermal stabilities (Mengel & Green, 1989; Wallace & Green, 1991). This means that the use of a more fertile bulk composition, instead of KLB-1, would yield relatively higher thermal stabilities of amphibole under water-undersaturated conditions. Finally, the presence of Ti in K-richterite increases its stability field to lower pressures and toward higher temperature (Konzett & Ulmer, 1999).

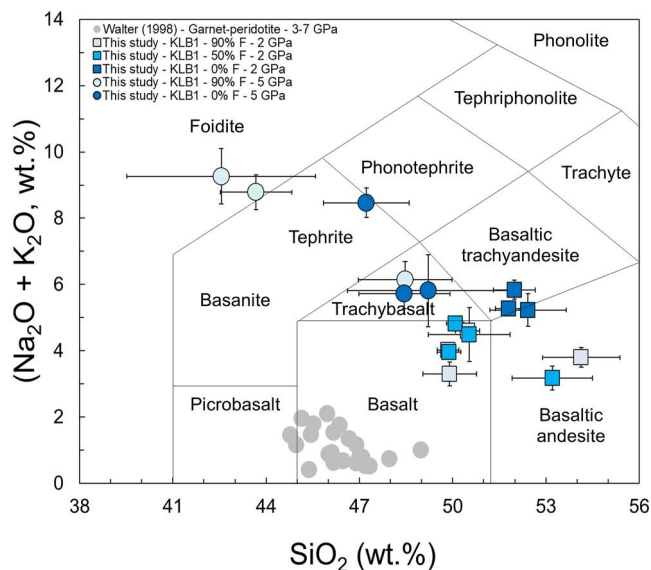


Figure 5. Summary of the chemical compositions of the silicate melts.

For phlogopite, the incorporation of only 1.6 wt.% F results in an increased stability of at least 5°C at 2 GPa (Figures 2 and 4). This effect is larger than reported in most previous studies that were run at lower pressures and for simplified and/or for chemically distinct bulk compositions (Figure 6). At 5 GPa, the enhanced stability of F-rich phlogopite compared to that of F-free phlogopite cannot be quantitatively constrained. However, the minimal difference between the decomposition temperatures derived for F-free and F-bearing phlogopite is consistent with the 2 GPa trend (Figure 6). Previous studies have shown that phlogopite from peridotitic xenoliths can contain up to 8 wt.% F (Liu et al., 2011), with examples from Sicily, Italy (Gianfagna et al., 2007) and Namalulu, Tanzania (Feneyrol et al., 2012) (see also Figure S1 in Supporting Information S1). Assuming that the effects of F on thermal stability are approximately linear, consistent with in situ observations at ambient pressures reported by Sun et al. (2022), the thermal stability could be increased by as much as ~222 and ~445°C for phlogopite containing 4 and 8 wt.%, respectively. Note that an approximately linear dependency of phlogopite thermal stability with F content is also consistent with the observations for simplistic natural systems obtained at 0.7–2.8 GPa (Dooley & Patiño Douce, 1996; Foley et al., 1986a; Hensen & Osanai, 1994). The

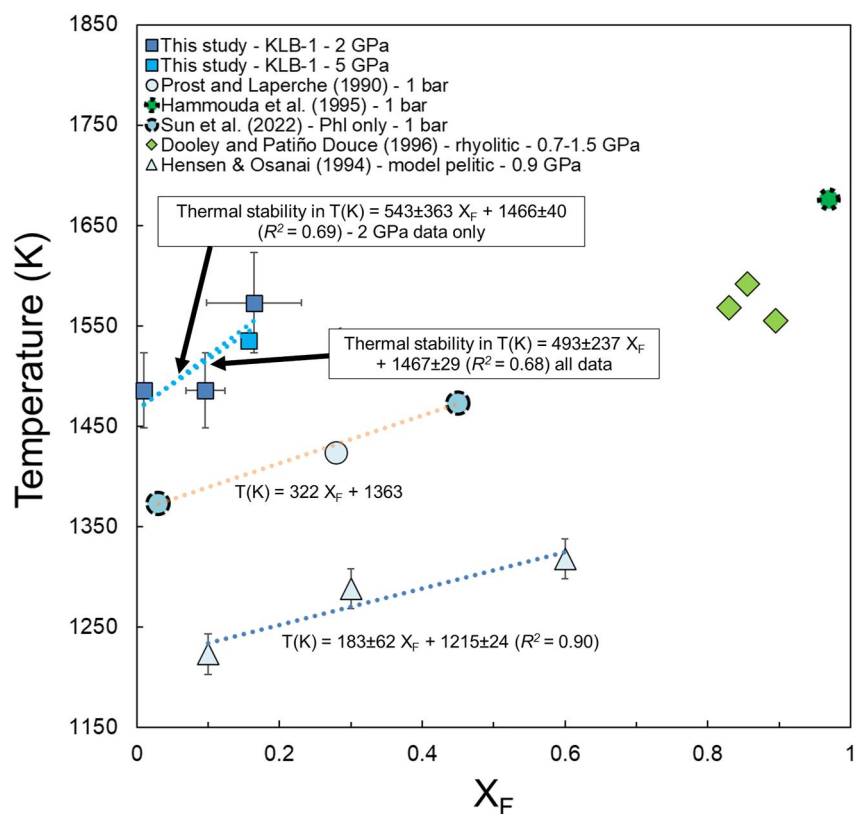


Figure 6. Thermal stabilities of phlogopite as a function of X_F , defined as $F/(F+OH)$, at different pressures, based on data from this study and previous work. Included for comparison purposes are 1 bar data (Hammouda et al., 1995; Prost & Laperche, 1990; Sun et al., 2022) and high-pressure data (0.7–1.5 GPa, Dooley & Patiño Douce, 1996; 0.9 GPa, Hensen & Osanai, 1994). Dashed lines represent fits to thermal stabilities that were derived for a single study at a constant pressure or at 2 and 5 GPa (this study, for comparative purposes).

estimated thermal stabilities of F-bearing phlogopite thus significantly exceeds previous estimates for F-free phlogopite of $<1,350^\circ\text{C}$ (Trønnes, 2002). Besides F, Fe and Ti may also affect the thermal stability of F-bearing phlogopite (Condamine et al., 2016; Motoyoshi & Hensen, 2001; Tareen et al., 1995, 1998). However, for Fe this is most likely an avoidance effect as the phlogopite Fe content decreases with F concentration (Munoz, 1984). Although the Ti content of phlogopite is generally positively correlated with F, the combination of both increases its stability considerably more than that would be expected for F or Ti alone, as implied from Ti-free F-KMASH experiments (Dooley & Patiño Douce, 1996). In addition, the phlogopite Ti content from natural samples and experiments varies greatly (e.g., Foley et al., 2022), which could explain some of the observed differences in thermal stabilities from previous studies. Our experimental results overall demonstrate that the important effects of F on phlogopite stability also occur in natural systems that are directly applicable to the terrestrial upper mantle and continental lithosphere.

4. Implications for F and OH Cycles of the Upper Mantle and Lithosphere

The observed stability of F-free and/or F-bearing K-richrichterite and phlogopite has important implications for the F and H cycles of the deeper Earth. We explore three different F contents of phlogopite, that is, 1.8, 4.5, and 8.1 wt. %. The effect of F on the thermal stability of phlogopite was assumed to be linear (Figure 6), consistent with currently derived thermal stabilities of phlogopite for different F content (see Section 3.3.4), and also to be constant with pressure. The validity of these assumptions needs to be explored in greater detail in future experimental work. Figures 7 and 8 show the modeled stabilities of K-richrichterite and phlogopite in a F-absent and F-rich system, with variable F contents, along different geothermal gradients (continental vs. oceanic).

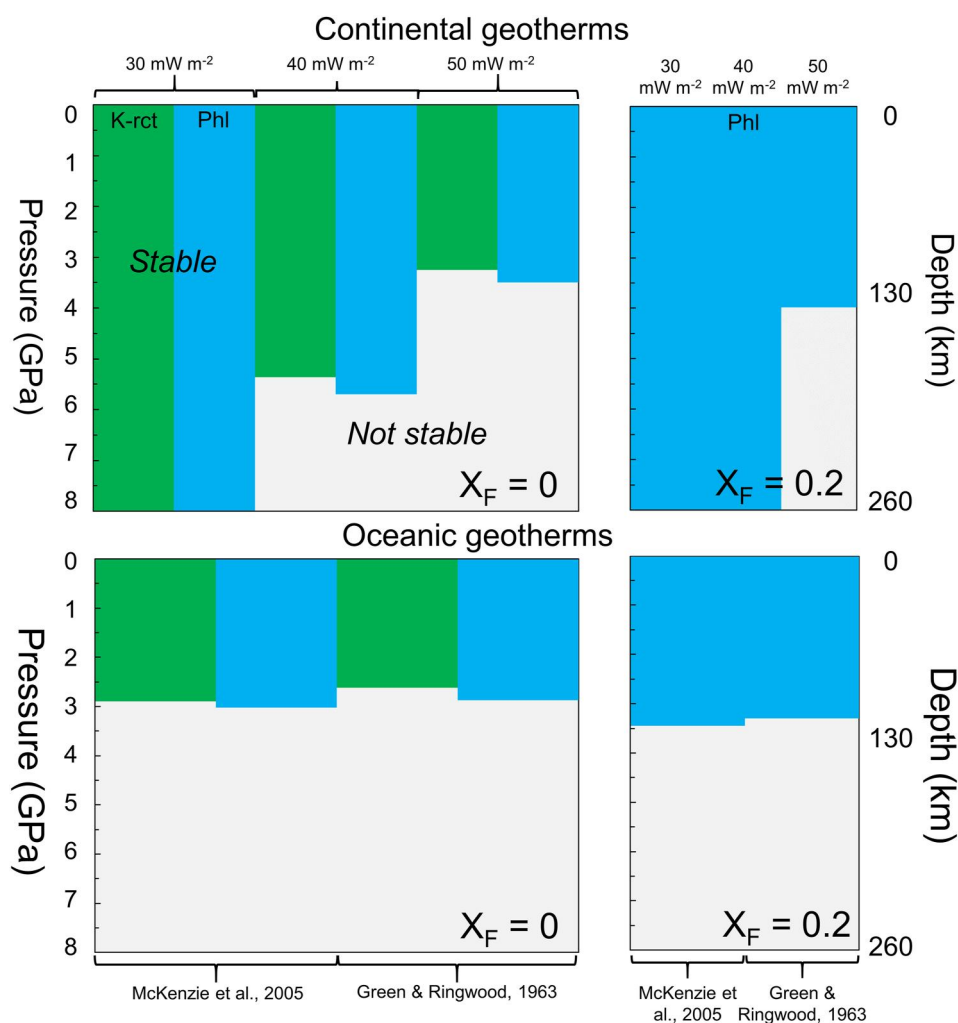


Figure 7. Modeled stabilities of K-richterite and phlogopite containing 0 or ~1.8 wt.% F (i.e., $X_F = 0$ or 0.20) along continental geotherms (assuming continental heat flows of 30, 40, or 50 mW m^{-2} ; Pollack & Chapman, 1977a, 1977b) and oceanic geotherms (Green & Ringwood, 1963; McKenzie et al., 2005) plotted as a function of pressure (GPa) and depth (km). The thermal stabilities of phlogopite were calculated using the fitted 2 GPa dependency from Figure 6. The thermal stabilities of K-richterite are plotted simply for reference purposes only in the $X_F = 0$ panel, as K-richterite is not affected by F within the resolution of our experimental work.

First, K-richterite is significantly less stable than F-bearing phlogopite at any F content and will readily decompose at relatively low P - T conditions (Figures 2–4). K-richterite is not expected to be stable at depths exceedingly approximately 110 km, corresponding to 3.25 GPa, for most considered geotherms, up to at least 240 km or ~8 GPa (Foley, 1991). At ~8 GPa, K-richterite reappears due to the destabilization of phlogopite (Frost, 2006 and references therein). As the presence of F seems to have little or no effect on K-richterite stability at 2 GPa in the KLB-1 composition, this conclusion remains likely valid for all considered scenarios. Both the F-free ($X_F = 0$) and 1.8 wt.% ($X_F = 0.2$) F-bearing phlogopite stability field generally does not extend to estimated upper mantle P - T conditions and those at greater depths (>200 km corresponding to 6 GPa). Only for the coldest continental geotherm, corresponding to a continental heat flow of 30 mW m^{-2} (i.e., very old cratons; Pollack & Chapman, 1977a, 1977b), phlogopite is stable beyond a depth of 200 km (Figure 7).

Extrapolation of the estimated stability for phlogopite with 4.5 and 8.1 wt.% F (i.e., $X_F = 0.5$ and 0.9), the latter as approximately the upper limit given the solubility of F in phlogopite (Edgar & Pizzolato, 1995; Sun et al., 2022), yields phlogopite stability that extends well beyond the continental lithosphere—asthenosphere boundary (Figure 8). For example, even within a hot oceanic regime phlogopite containing >4.5 wt.% F ($X_F = 0.5$) would be stable to depths of up to 130 km. In continental lithosphere, phlogopite with 4.5 wt.% F would be stable at depths

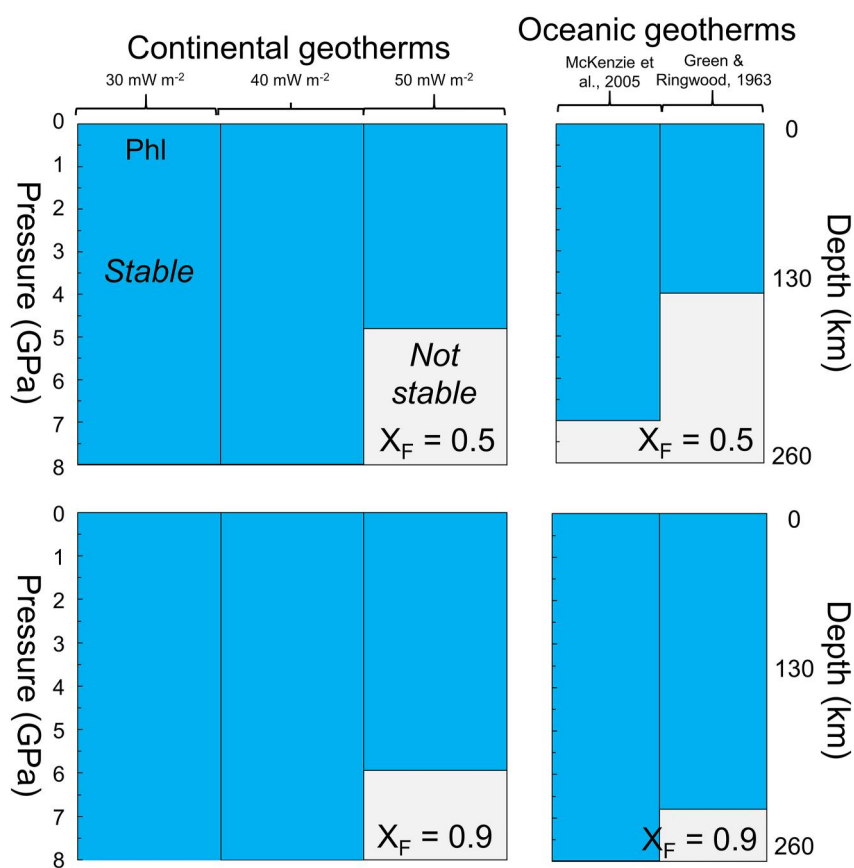


Figure 8. Modeled stabilities of K-richterite and phlogopite containing ~4.5 or 8.1 wt.% F (i.e., $X_F = 0.5$ or $X_F = 0.9$) along continental geotherms (assuming continental heat flows of 30, 40, or 50 mW m^{-2} ; Pollack & Chapman, 1977a, 1977b) and oceanic geotherms (Green & Ringwood, 1963; McKenzie et al., 2005) plotted as a function of pressure (GPa) and depth (km). See Figure 7 caption for additional details.

of >155 km, a trend which greatly increases with age of the continental crust (i.e., cooler geotherms) and increasing X_F of phlogopite (Figure 7). These calculations show that F-bearing phlogopite is an extremely efficient fluorine and hydrogen reservoir in the continental lithosphere. The longevity of F and H storage through phlogopite is likely profound, as only significant regional heating, for example, through continental rifting and/or break-up, would be sufficient to decompose phlogopite stable within these domains. Continuing metasomatism of the continental lithosphere through time will increase the F content of phlogopite present within the lithosphere, thereby increasing its stability. The degree of H storage would obviously depend on the F content of the phlogopite, as they both occupy the hydroxyl site.

The preferential incorporation of F over OH due to the more compatible behavior of F in phlogopite will yield a continuous increase of the F/OH ratio of the phlogopite during partial melting. In turn, this will further increase the stability of phlogopite, thereby acting as an efficient F sink within the upper mantle. This is expected to continue until most OH is replaced by F in the phlogopite (i.e., ~8 wt.% F), maximizing its thermal stability. Finally, due to the F-Fe avoidance observed in phlogopite (Figure S6 in Supporting Information S1), a higher initial FeO content of phlogopite will lower F solubility. Higher initial FeO will therefore reduce the maximum effects of F on phlogopite thermal stability.

5. Conclusions

New high P-T experiments were used to constrain the effects of F on K-richterite and phlogopite stability in natural systems. K-richterite was found to be stable only at the lowest P-T conditions considered (<1,175°C at 2 GPa), independent of the amount of F. The thermal stability of phlogopite in natural systems significantly increases by the addition of F, with an estimated increase of ~55°C/wt.% F. These large effects of F on the thermal

stability of phlogopite indicates that phlogopite can be stabilized at depths much greater than 250 km in very old, thick continental crust. Fluorine-rich phlogopite stability also extends to at least 130 km depth in oceanic lithosphere, depending on the geotherm and F content considered. This shows that F-rich phlogopite is a major carrier of F, H, and other volatiles which can be only decomposed in major regional volcanic events, such as rifting or continental break-up.

Data Availability Statement

Raw experimental data are publicly available in Steenstra (2024).

Acknowledgments

We thank Maik Trogisch for excellent sample preparation and Beate Schmitte for her valuable assistance in conducting EPMA analyses. We also thank A. Lanati for helpful advice related to the experiments. E.S.S. was funded through Marie Curie Postdoctoral Fellowship 101020611. M.K. was funded through a Humboldt Fellowship. The study was also partially supported by the SFB TRR-170 Grant. We thank three anonymous reviewers for their constructive comments on this manuscript.

References

- Ballhaus, C. (1993). Redox states of lithospheric and asthenospheric upper mantle. *Contributions to Mineralogy and Petrology*, 114(3), 331–348. <https://doi.org/10.1007/bf01046536>
- Bekaert, D. V., Turner, S. J., Broadley, M. W., Barnes, J. D., Halldorsson, S. A., Labidi, J., et al. (2021). Subduction-driven volatile recycling: A Global mass balance. *Annual Review of Earth and Planetary Sciences*, 49(1), 37–70. <https://doi.org/10.1146/annurev-earth-071620-055024>
- Beyer, C., Klemme, S., Grützner, T., Ireland, T., Magee, C. W., & Frost, D. J. (2016). Fluorine partitioning between eclogitic garnet, clinopyroxene, and melt at upper mantle conditions. *Chemical Geology*, 437, 88–97. <https://doi.org/10.1016/j.chemgeo.2016.05.032>
- Blundy, J., Melekhova, E., Zibera, L., Humphreys, M. C. S., Cerantola, V., Brooker, R. A., et al. (2020). Effect of redox on Fe-Mg-Mn exchange between olivine and melt and an oxybarometer for basalts. *Contributions to Mineralogy and Petrology*, 175(11), 103. <https://doi.org/10.1007/s00410-020-01736-7>
- Bose, K., & Ganguly, J. (1995). Quartz-coesite transition revisited: Reversed experimental determination at 500–1200°C and retrieved thermochemical properties. *American Mineralogist*, 80(3–4), 231–238. <https://doi.org/10.2138/am-1995-3-404>
- Condamine, P., & Médard, E. (2014). Experimental melting of phlogopite-bearing mantle at 1 GPa: Implications for potassic magmatism. *Earth and Planetary Science Letters*, 397, 80–92. <https://doi.org/10.1016/j.epsl.2014.04.027>
- Condamine, P., Médard, E., & Devidal, J. L. (2016). Experimental melting of phlogopite-peridotite in the garnet stability field. *Contributions to Mineralogy and Petrology*, 171(11), 95. <https://doi.org/10.1007/s00410-016-1306-0>
- Dai, L., & Karato, S. (2009). Electrical conductivity of orthopyroxene: Implications for the water content of the asthenosphere. *Proceedings of the Japan Academy, series B*, 85(10), 466–475. <https://doi.org/10.2183/pjab.85.466>
- Dasgupta, R., Hirschmann, M. M., & Smith, N. D. (2007). Partial melting experiments of peridotite + CO₂ at 3 GPa and genesis of alkalic ocean Island basalts. *Journal of Petrology*, 48(11), 2093–2124. <https://doi.org/10.1093/petrology/egm053>
- Davis, F. A., Tangeman, J. A., Tenner, T. J., & Hirschmann, M. M. (2009). The composition of KLB-1 peridotite. *American Mineralogist*, 94(1), 176–180. <https://doi.org/10.2138/am.2009.2984>
- Dawson, J. B., & Smith, J. V. (1977). The MARID (mica-amphibole-rutile-ilmenite-diopside) suite of xenoliths in kimberlite. *Geochimica et Cosmochimica Acta*, 41(2), 309–310. [https://doi.org/10.1016/0016-7037\(77\)90239-3](https://doi.org/10.1016/0016-7037(77)90239-3)
- Dooley, D. F., & Patiño Douce, A. E. (1996). Vapor-absent melting of F- and Ti-rich phlogopite + quartz: effects on phlogopite stability and melt compositions. *American Mineralogist*, 81(1–2), 202–212. <https://doi.org/10.2138/am-1996-1-225>
- Edgar, A. D., & Pizzolato, L. A. (1995). An experimental study of partitioning of fluorine between K-richterite, apatite, phlogopite, and melt at 20 kbar. *Contributions to Mineralogy and Petrology*, 121(3), 247–257. <https://doi.org/10.1007/bf02688240>
- Edgar, A. D., Pizzolato, L. A., & Sheen, J. (1996). Fluorine in igneous rocks and minerals with emphasis on ultrapotassic mafic and ultramafic magmas and their mantle source regions. *Mineralogical Magazine*, 60, 243–257. <https://doi.org/10.1180/minmag.1996.060.399.01>
- Edgar, A. D., Vukadinovic, D., & Lloyd, F. E. (1991). Distribution of fluorine between minerals and glass in lamproites, lamprophyres and kamafugites: Implications for the role of F in deep mantle-derived magmas. In *Extended Abstracts, 5th International Kimberlite Conference Araxa Brazil* (pp. 79–81).
- Exley, R. A., & Smith, J. V. (1982). The role of apatite in mantle enrichment processes and in the petrogenesis of some alkali basalt suites. *Geochimica et Cosmochimica Acta*, 46(8), 1375–1384. [https://doi.org/10.1016/0016-7037\(82\)90273-3](https://doi.org/10.1016/0016-7037(82)90273-3)
- Ezad, I. S., & Foley, S. F. (2022). Experimental partitioning of fluorine and barium in lamproites. *American Mineralogist*, 107(11), 2008–2019. <https://doi.org/10.2138/am-2022-8289>
- Fedortchouk, Y., Lieske, C., & McCammon, C. (2019). Diamond destruction and growth during mantle metasomatism: An experimental study of diamond resorption features. *Earth and Planetary Science Letters*, 506, 493–506. <https://doi.org/10.1016/j.epsl.2018.11.025>
- Feneyrol, J., Giuliani, G., Ohnenstetter, D., Rollion-Bard, C., Robert, J. L., & Malisa, E. P. J. (2012). Evidence of evaporates in the genesis of the vanadian grossular ‘tsavorite’ deposit in Namalulu, Tanzania. *The Canadian Mineralogist*, 50(3), 745–769. <https://doi.org/10.3749/canmin.50.3.745>
- Flemetakis, S., Berndt, J., Klemme, S., Genske, F., Cadoux, A., Louvel, M., & Rohrbach, A. (2020). An improved electron microprobe method for the analysis of halogens in natural silicate glasses. *Microscopy and Microanalytics*, 26(5), 857–866. <https://doi.org/10.1017/s1431927620013495>
- Flemetakis, S., Klemme, S., Stracke, A., Genske, F., Berndt, J., & Rohrbach, A. (2021). Constraining the presence of amphibole and mica in metasomatized mantle sources through halogen partitioning experiments. *Lithos*, 380, 105859. <https://doi.org/10.1016/j.lithos.2020.105859>
- Flemetakis, S., Tiraboschi, C., Rohrbach, A., Berndt, J., & Klemme, S. (2022). The stability of antigorite in subduction zones revisited: The effect of F on antigorite stability and its breakdown reactions at high pressures and temperatures, with implications for the geochemical cycles of halogens. *Contributions to Mineralogy and Petrology*, 177(7), 70. <https://doi.org/10.1007/s00410-022-01934-5>
- Foley, S. F. (1991). High-pressure stability of the fluor- and hydroxy-endmembers of pargasite and K-richterite. *Geochimica et Cosmochimica Acta*, 55(9), 2689–2694. [https://doi.org/10.1016/0016-7037\(91\)90386-j](https://doi.org/10.1016/0016-7037(91)90386-j)
- Foley, S. F., Ezad, I. S., van der Laan, S. R., & Pertermann, M. (2022). Melting of hydrous pyroxenites with alkali amphiboles in the continental mantle: 1. Melting relations and major element compositions of melts. *Geoscience Frontiers*, 13(4), 101380. <https://doi.org/10.1016/j.gsf.2022.101380>
- Foley, S. F., Taylor, W. R., & Green, D. H. (1986a). The effect of fluorine on phase relationships in the system KAlSiO₄-Mg₂SiO₄-SiO₂ and the solution mechanism of fluorine in silicate melts. *Contributions to Mineralogy and Petrology*, 93(1), 46–55. <https://doi.org/10.1007/bf00963584>

- Foley, S. F., Taylor, W. R., & Green, D. H. (1986b). The role of fluorine and oxygen fugacity in the genesis of the ultrapotassic rocks. *Contributions to Mineralogy and Petrology*, 94(2), 183–192. <https://doi.org/10.1007/bf00592935>
- Frost, D. J. (2006). The stability of hydrous mantle phases. *Reviews in Mineralogy and Geochemistry*, 62(1), 243–271. <https://doi.org/10.2138/rmg.2006.62.11>
- Frost, D. J., & Wood, B. J. (1997). Experimental measurements of the fugacity of CO₂ and graphite/diamond stability from 35 to 77 kbar at 925 to 1650°C. *Geochimica et Cosmochimica Acta*, 61(8), 1565–1574. [https://doi.org/10.1016/s0016-7037\(97\)00035-5](https://doi.org/10.1016/s0016-7037(97)00035-5)
- Fumagalli, P., & Klemme, S. (2015). Mineralogy of the Earth: Phase transitions and mineralogy of the upper mantle. In *Treatise on geophysics* (2nd ed., pp. 7–31). <https://doi.org/10.1016/B978-0-444-53802-4.00052-X>
- Gervasoni, F., Klemme, S., Rohrbach, A., Grützner, T., & Berndt, J. (2017). Experimental constraints on mantle metasomatism caused by silicate and carbonate melts. *Lithos*, 282–283, 173–186. <https://doi.org/10.1016/j.lithos.2017.03.004>
- Ghosh, S., Litasov, K., & Ohtani, E. (2014). Phase relations and melting of carbonated peridotite between 10 and 20 GPa: A proxy for alkali- and CO₂-rich silicate melts in the deep mantle. *Contributions to Mineralogy and Petrology*, 167(2), 964. <https://doi.org/10.1007/s00410-014-0964-z>
- Gianfagna, A., Scordari, F., Mazziotti-Tagliani, M., Ventrucci, G., & Ottolini, L. (2007). Fluorophlogopite from Biancavilla (Mt. Etna, Sicily, Italy): Crystal structure and crystal chemistry of a new F-dominant analog of phlogopite. *American Mineralogist*, 92(10), 1601–1609. <https://doi.org/10.2138/am.2007.2502>
- Green, D. H., Hibberson, W. O., Kovács, I., & Rosenthal, A. (2010). Water and its influence on the lithosphere–asthenosphere boundary. *Nature*, 467(7314), 448–451. <https://doi.org/10.1038/nature09369>
- Green, D. H., & Ringwood, A. E. (1963). Mineral assemblages in a model mantle composition. *Journal of Geophysical Research*, 68, 937–945.
- Gregoire, M., Bell, D. R., & Roux, A. P. L. (2002). Trace element geochemistry of phlogopite-rich mafic mantle xenoliths: Their classification and their relationship to phlogopite-bearing peridotites and kimberlites revisited. *Contributions to Mineralogy and Petrology*, 142(5), 603–625. <https://doi.org/10.1007/s00410-001-0315-8>
- Grützner, T., Kohn, S. C., Bromiley, D. W., Rohrbach, A., Berndt, J., & Klemme, S. (2017). The storage capacity of fluorine in olivine and pyroxene under upper mantle conditions. *Geochimica et Cosmochimica Acta*, 208, 160–170. <https://doi.org/10.1016/j.gca.2017.03.043>
- Hammouda, T., Pichavant, M., Barbey, P., & Brearley, A. (1995). Synthesis of fluorophlogopite single crystals. Applications to experimental studies. *European Journal of Mineralogy*, 7(6), 1381–1387. <https://doi.org/10.1127/ejm/7/6/1381>
- Hecker, J. G., Marks, M. A. W., Wenzel, T., & Markl, G. (2020). Halogens in amphibole and mica from mantle xenoliths: Implications for the halogen distribution and halogen budget of the metasomatized continental lithosphere. *American Mineralogist*, 105(6), 781–794. <https://doi.org/10.2138/am-2020-7174>
- Hensen, B. J., & Osanai, Y. (1994). Experimental study of dehydration melting of F-bearing biotite in model pelitic compositions. *Mineralogical Magazine*, 58A(1), 410–411. <https://doi.org/10.1180/minmag.1994.58a.1.214>
- Hirose, K., & Kawamoto, T. (1995). Hydrous partial melting of lherzolite at 1 GPa: The effect of H₂O on the genesis of basaltic magmas. *Earth and Planetary Science Letters*, 133(3–4), 463–473. [https://doi.org/10.1016/0012-821x\(95\)00096-u](https://doi.org/10.1016/0012-821x(95)00096-u)
- Holloway, J. R., & Ford, C. E. (1975). Fluid-absent melting of the fluoro-hydroxy amphibole pargasite to 35 kilobars. *Earth and Planetary Science Letters*, 25(1), 44–48. [https://doi.org/10.1016/0012-821x\(75\)90208-3](https://doi.org/10.1016/0012-821x(75)90208-3)
- Jaques, A. L., Lewis, J. D., Smith, C. B., Gregory, G. P., Ferguson, J., Chappell, B. W., & McCulloch, M. T. (1984). The diamond bearing ultrapotassic (lamproitic) rocks of the West Kimberley region, Western Australia. In J. Kornprobst (Ed.), *Kimberlites I: Kimberlites and related rocks* (pp. 225–254).
- Kawamoto, T. (2004). Hydrous phase stability and partial melt chemistry in H₂O-saturated KLB-1 peridotite up to the uppermost lower mantle conditions. *Physics of the Earth and Planetary Interiors*, 143–144, 387–395. [https://doi.org/10.1016/s0031-9201\(04\)00070-6](https://doi.org/10.1016/s0031-9201(04)00070-6)
- Klemme, S., & O'Neill, H. S. C. (1997). The reaction MgCr₂O₄ + SiO₂ = Cr₂O₃ + MgSiO₃ and the free energy formation of magnesiochromite (MgCr₂O₄). *Contributions to Mineralogy and Petrology*, 130(1), 59–65. <https://doi.org/10.1007/s004100050349>
- Klemme, S., & Stalder, R. (2018). Halogens in the Earth's mantle: What we know and what we don't. In *The role of halogens in terrestrial and extraterrestrial geochemical processes* (Vol. 847–869). Springer.
- Knibbe, J. S., Luginbühl, S. M., Stoevelaar, R., van der Plas, W., van Harlingen, D. M., Rai, N., et al. (2018). Calibration of a multi-anvil high-pressure apparatus to simulate planetary interior conditions. *EPJ Techniques & Instrumentation*, 5(1), 5. <https://doi.org/10.1140/epjti/s40485-018-0047-z>
- Konzett, J. (1997). Phase relations and chemistry of Ti-rich K-richterite-bearing mantle assemblages: An experimental study to 8.0 GPa in a Ti-KNCMASH system. *Contributions to Mineralogy and Petrology*, 128(4), 385–404. <https://doi.org/10.1007/s004100050316>
- Konzett, J., & Frost, D. J. (2009). The high *P-T* stability of hydroxyl-apatite in natural and simplified MORB—An experimental study to 15 GPa with implications for transport and storage of phosphorus and halogens in subduction zones. *Journal of Petrology*, 50(11), 2043–2062. <https://doi.org/10.1093/ptrology/egp068>
- Konzett, J., Rhede, D., & Frost, D. J. (2012). The high *PT* stability of apatite and Cl partitioning between apatite and hydrous potassic phases in peridotite: An experimental study to 19 GPa with implications for the transport of P, Cl and K in the upper mantle. *Contributions to Mineralogy and Petrology*, 163(2), 277–296. <https://doi.org/10.1007/s00410-011-0672-x>
- Konzett, J., & Ulmer, P. (1999). The stability of hydrous potassic phases in lherzolitic mantle—An experimental study to 9.5 GPa in simplified and natural bulk compositions. *Journal of Petrology*, 40(4), 629–652. <https://doi.org/10.1093/ptrology/40.4.629>
- Leshner, C. E., & Walker, D. (1988). Cumulate maturation and melt migration in a temperature gradient. *Journal of Geophysical Research*, 93(B9), 10295–10311. <https://doi.org/10.1029/jb093ib09p10295>
- Liu, C.-Z., Wu, F.-Y., Chung, S.-L., & Zhao, Z.-D. (2011). Fragments of hot and metasomatized mantle lithosphere in Middle Miocene ultrapotassic lavas, southern Tibet. *Geology*, 39(10), 923–926. <https://doi.org/10.1130/g32172.1>
- McDonough, W. F., & Sun, S.-S. (1995). The composition of the Earth. *Chemical Geology*, 120(3–4), 223–253. [https://doi.org/10.1016/0009-2541\(94\)00140-4](https://doi.org/10.1016/0009-2541(94)00140-4)
- McKenzie, D., Jackson, J., & Priestley, K. (2005). Thermal structure of oceanic and continental lithosphere. *Earth and Planetary Science Letters*, 233(3–4), 337–349. <https://doi.org/10.1016/j.epsl.2005.02.005>
- Mengel, K., & Green, D. H. (1989). Stability of amphibole and phlogopite in metasomatized peridotite under water-saturated and water-undersaturated conditions. In *IV International Kimberlite Conference, Australian Journal of Earth Science Special Publications* (Vol. 14, pp. 571–581).
- Motoyoshi, Y., & Hensen, B. J. (2001). F-rich phlogopite stability in ultra-high-temperature metapelites from the Napier Complex, East Antarctica. *American Mineralogist*, 86(11–12), 1404–1413. <https://doi.org/10.2138/am-2001-11-1209>
- Munoz, J. L. (1984). F-OH and Cl-OH exchange in micas with applications to hydrothermal ore deposits. In S. W. Bailey (Ed.), *Micas. Reviews in mineralogy* (Vol. 13, pp. 469–493).

- Niida, K., & Green, D. H. (1999). Stability and chemical composition of pargasitic amphibole in MORB pyroxene under upper mantle conditions. *Contributions to Mineralogy and Petrology*, 135(1), 18–40. <https://doi.org/10.1007/s004100050495>
- Palme, H., & O'Neill, H. S. C. (2014). Cosmochemical estimates of mantle composition. In H. D. H. K. Turekian (Ed.), *Treatise on geochemistry* (pp. 1–39).
- Petersen, E. U., Essene, E. J., & Peacor, D. R. (1982). Fluorine end-member micas and amphiboles. *American Mineralogist*, 67(5–6), 538–544.
- Peterson, J. W., Chacko, T., & Kuehner, S. M. (1991). The effects of fluorine on the vapor-absent melting of phlogopite + quartz: Implications for deep-crustal processes. *American Mineralogist*, 76, 470–476.
- Pintér, Z., Foley, S. F., Yaxley, G. M., Rosenthal, A., Papp, R. P., Lanati, A. W., & Rushmer, T. (2021). Experimental investigation of the composition of incipient melts in upper mantle peridotites in the presence of CO₂ and H₂O. *Lithos*, 396–397, 106224. <https://doi.org/10.1016/j.lithos.2021.106224>
- Pollack, H. N., & Chapman, D. S. (1977a). On the regional variation of heat flow, geotherms and lithosphere thickness. *Tectonophysics*, 38(3–4), 279–296. [https://doi.org/10.1016/0040-1951\(77\)90215-3](https://doi.org/10.1016/0040-1951(77)90215-3)
- Pollack, H. N., & Chapman, D. S. (1977b). Mantle heat flow. *Earth and Planetary Science Letters*, 34(2), 174–184. [https://doi.org/10.1016/0012-821x\(77\)90002-4](https://doi.org/10.1016/0012-821x(77)90002-4)
- Presnall, D. C., Dixon, S. A., Dixon, J. R., O'Donnell, T. H., Brenner, N. L., Schrock, R. L., & Dycus, D. W. (1978). Liquidus phase relations on the join diopside-forsterite-anorthite from 1 atm. To 20 kbar: Their bearing on the generation and crystallization of basaltic magma. *Contributions to Mineralogy and Petrology*, 66(2), 203–220. <https://doi.org/10.1007/bf00372159>
- Prost, R., & Laperche, V. (1990). Far-infrared study of potassium in micas. *Clays and Clay Minerals*, 38(4), 351–355. <https://doi.org/10.1346/ccmn.1990.0380403>
- Roeder, P. L., & Emslie, R. F. (1970). Olivine-liquid equilibrium. *Contributions to Mineralogy and Petrology*, 29(4), 275–289. <https://doi.org/10.1007/bf00371276>
- Sorbadere, F., Laurenz, V., Frost, D. J., Wenz, M., Rosenthal, A., McCammon, C., & Rivard, C. (2018). The behaviour of ferric iron during partial melting of peridotite. *Geochimica et Cosmochimica Acta*, 239, 235–254. <https://doi.org/10.1016/j.gca.2018.07.019>
- Sorbadere, F., Médard, E., Laporte, D., & Schiano, P. (2013). Experimental melting of hydrous peridotite-pyroxenite mixed sources: Constraints on the genesis of silica-undersaturated magmas beneath volcanic arcs. *Earth and Planetary Science Letters*, 384, 42–56. <https://doi.org/10.1016/j.epsl.2013.09.026>
- Steenstra, E. S. (2024). Thermal stability of F-rich phlogopite and K-rich richterite during partial melting of metasomatized mantle peridotite with implications for deep Earth volatile cycles [Dataset]. Mendeley Data, V3. <https://doi.org/10.17632/fxghs2gxp.3>
- Steenstra, E. S., van Haaster, F., van Mulligen, R., Fletmetakis, S., Berndt, J., Klemme, S., & van Westrenen, W. (2020). An experimental assessment of the chalcophile behavior of F, Cl, Br, and I: Implications for the fate of halogens during planetary accretion and the formation of magmatic ore deposits. *Geochimica et Cosmochimica Acta*, 273, 275–290. <https://doi.org/10.1016/j.gca.2020.01.006>
- Straub, S. M., & Layne, G. D. (2003). The systematics of chlorine, fluorine, and water in Izu arc front volcanic rocks: Implications for volatile recycling in subduction zones. *Geochimica et Cosmochimica Acta*, 67(21), 4179–4203. [https://doi.org/10.1016/s0016-7037\(03\)00307-7](https://doi.org/10.1016/s0016-7037(03)00307-7)
- Sudo, A., & Tatsumi, Y. (1990). Phlogopite and K-amphibole in the upper mantle: Implication for magma generation in subduction zones. *Geophysical Research Letters*, 17(1), 29–32. <https://doi.org/10.1029/g1017i001p00029>
- Sun, J., Yang, Y., Ingrin, J., Wang, Z., & Xia, Q. (2022). Impact of fluorine on the thermal stability of phlogopite. *American Mineralogist*, 107(5), 815–825. <https://doi.org/10.2138/am-2022-8051>
- Susaki, J., Akaogi, M., Akimoto, S., & Shimomura, O. (1985). Garnet-perovskite transformation in CaGeO₃—In situ X-ray measurements using synchrotron radiation. *Geophysical Research Letters*, 12(10), 729–732. <https://doi.org/10.1029/g1012i010p00729>
- Takahashi, E. (1986). Melting of a dry peridotite KLB-1 up to 14 GPa: Implications on the origin of peridotitic upper mantle. *Journal of Geophysical Research*, 91(B9), 9367–9382. <https://doi.org/10.1029/jb091ib09p09367>
- Tareen, J. A. K., Keshava Prasad, A. V., Basavalingu, B., & Ganesha, A. V. (1995). The effect of fluorine and titanium on vapour-absent melting of phlogopite and quartz. *Mineralogical Magazine*, 59(396), 566–570. <https://doi.org/10.1180/minmag.1995.059.396.19>
- Tareen, J. A. K., Keshava Prasad, A. V., Basavalingu, B., & Ganesha, A. V. (1998). Stability of F-Ti phlogopite in the system phlogopite–Sillimanite–Quartz: An experimental study of dehydration melting in H₂O-saturated and undersaturated conditions. *Mineralogical Magazine*, 62(3), 373–380. <https://doi.org/10.1180/0026464198547774>
- Trønnes, R. G. (2002). Stability range and decomposition of potassic richterite and phlogopite end members at 5–15 GPa. *Mineralogy and Petrology*, 74(2–4), 129–148. <https://doi.org/10.1007/s007100200001>
- Trønnes, R. G., Takahashi, E., & Scarfe, C. M. (1988). Stability of K-rich richterite and phlogopite to 14 GPa. *Transactions American Geophysical Union*, 69, 1510–1511.
- Van den Bleeken, G., & Koga, K. T. (2015). Experimentally determined distribution of fluorine and chlorine upon hydrous slab melting, and implications for F-Cl cycling through subduction zones. *Geochimica et Cosmochimica Acta*, 171, 353–373. <https://doi.org/10.1016/j.gca.2015.09.030>
- Van Kan Parker, M., Mason, P. R. D., & van Westrenen, W. (2011). Experimental study of trace element partitioning between lunar orthopyroxene and anhydrous silicate melt: Effects of lithium and iron. *Chemical Geology*, 285(1–4), 1–14. <https://doi.org/10.1016/j.chemgeo.2011.02.007>
- Van Westrenen, W., van Orman, J. A., Watson, H., Fei, Y., & Watson, E. B. (2003). Assessment of temperature gradients in multi-anvil assemblies using spinel layer growth kinetics. *Geochemistry, Geophysics, Geosystems*, 4, 1036. <https://doi.org/10.1029/2002GC000474>
- Vukadinovic, D., & Edgar, A. D. (1993). Phase relations in the phlogopite-apatite system at 20 kbar; implications for the role of fluorine in mantle melting. *Contributions to Mineralogy and Petrology*, 114(2), 247–254. <https://doi.org/10.1007/bf00307759>
- Wallace, M. E., & Green, D. H. (1991). The effect of bulk rock composition on the stability of amphibole in the upper mantle: Implications for solidus positions and mantle metasomatism. *Mineralogy and Petrology*, 44(1–2), 1–19. <https://doi.org/10.1007/bf01167097>
- Walter, M. J. (1998). Melting of garnet peridotite and the origin of Komatiite and depleted lithosphere. *Journal of Petrology*, 39(1), 29–60. <https://doi.org/10.1093/ptrology/39.1.29>
- Walter, M. J. (2003). Melt extraction and compositional variability in mantle lithosphere. *Treatise on geochemistry*, 2, 568.
- Wang, J., Takahashi, E., Xiong, X., Chen, L., Li, L., Suzuki, T., & Walter, M. J. (2020). The water-saturated solidus and second critical endpoint of peridotite: Implications for magma genesis within the mantle wedge. *Journal of Geophysical Research: Solid Earth*, 125(8), e2020JB019452. <https://doi.org/10.1029/2020jb019452>
- Watson, E. B., Wark, D. A., Price, J. D., & van Orman, J. A. (2002). Mapping the thermal structure of solid-media pressure assemblies. *Contributions to Mineralogy and Petrology*, 142(6), 640–652. <https://doi.org/10.1007/s00410-001-0327-4>
- Wyllie, P. J. (1987). Discussion of recent papers on carbonated peridotite, bearing on mantle metasomatism and magmatism. *Earth and Planetary Science Letters*, 82(3–4), 391–397. [https://doi.org/10.1016/0012-821x\(87\)90213-5](https://doi.org/10.1016/0012-821x(87)90213-5)

- Yoder, H. S., & Eugster, H. P. (1954). Phlogopite synthesis and stability range. *Geochimica et Cosmochimica Acta*, 6(4), 157–185. [https://doi.org/10.1016/0016-7037\(54\)90049-6](https://doi.org/10.1016/0016-7037(54)90049-6)
- Zhang, C., Koepke, J., Wang, L.-X., Wolff, P. E., Wilke, S., Stechern, A., et al. (2016). A practical method for accurate measurement of trace level fluorine in Mg- and Fe-bearing minerals and glasses using electron probe microanalysis. *Geostandards and Geoanalytical Research*, 40(3), 351–363. <https://doi.org/10.1111/j.1751-908x.2015.00390.x>
- Zhang, Y., Liang, X., Wang, C., Jin, Z., Zhu, L., & Gan, W. (2020). Experimental constraints on the partial melting of sediment-metasomatized lithospheric mantle in subduction zones. *American Mineralogist*, 105(8), 1191–1203. <https://doi.org/10.2138/am-2020-7403>

References From the Supporting Information

- Aradi, L. E., Bali, E., Patko, L., Hidas, K., Kovacs, I. J., Zanetti, A., et al. (2020). Geochemical evolution of the lithospheric mantle beneath the Styrian basin (Western Pannonian basin). *Lithos*, 378–379, 105831. <https://doi.org/10.1016/j.lithos.2020.105831>
- Boettcher, A. L., & O'Neil, J. R. (1980). Stable isotope, chemical, and petrographic studies of high-pressure amphiboles and micas: Evidence for metasomatism in the mantle source regions of alkali basalts and kimberlites. *American Journal of Science*, 280-A, 594–621.
- Canil, D., & Scarfe, C. M. (1989). Origin of phlogopite in mantle xenoliths from Kostal lake, wells Gray Park, British Columbia. *Journal of Petrology*, 30(5), 1159–1179. <https://doi.org/10.1093/ptrology/30.5.1159>
- Carswell, D. A. (1975). Primary and secondary phlogopites and clinopyroxenes in garnet lherzolite xenoliths. *Physics and Chemistry of the Earth*, 9, 417–429. [https://doi.org/10.1016/0079-1946\(75\)90031-2](https://doi.org/10.1016/0079-1946(75)90031-2)
- Casagli, A., Frezzotti, M.-L., Peccerillo, A., Tiepolo, M., & De Astis, G. (2017). (Garnet)-Spinel Peridotite Xenoliths from Mega (Ethiopia): Evidence for rejuvenation and dynamic thinning of the lithosphere beneath the southern main Ethiopian Rift. *Chemical Geology*, 455, 231–248. <https://doi.org/10.1016/j.chemgeo.2016.11.001>
- Coticelli, S., & Peccerillo, A. (1990). Petrological significance of high-pressure ultramafic xenoliths from ultrapotassic rocks of central Italy. *Lithos*, 24(4), 305–322. [https://doi.org/10.1016/0024-4937\(89\)90050-9](https://doi.org/10.1016/0024-4937(89)90050-9)
- Downes, H., MacDonald, R., Upton, B. G. J., Cox, K. G., Bodinier, J. L., Mason, P. R. D., et al. (2004). Ultramafic xenoliths from the Bearpaw Mountains, Montana, USA: Evidence for multiple metasomatic events in the lithospheric mantle beneath the Wyoming Craton. *Journal of Petrology*, 45(8), 1631–1662. <https://doi.org/10.1093/ptrology/egh027>
- Doyle, P. M., Bell, D. R., & Le Roex, A. P. (2004). Fine-grained pyroxenites from the Gansfontein kimberlite, South Africa: Evidence for megacryst magma—Mantle interaction. *South African Journal of Geology*, 107(1–2), 285–300. <https://doi.org/10.2113/107.1-2.285>
- Draper, D. S. (1992). Spinel lherzolite xenoliths from Lorena butte, Simcoe Mountains, southern Washington (USA). *The Journal of Geology*, 100(6), 766–775. <https://doi.org/10.1086/629627>
- Franz, L., Becker, K.-P., Kramer, W., & Herzig, P. M. (2002). Metasomatic mantle xenoliths from the Bismarck Microplate (Papua New Guinea) —Thermal evolution, geochemistry and extent of slab-induced metasomatism. *Journal of Petrology*, 43(2), 315–343. <https://doi.org/10.1093/ptrology/43.2.315>
- Frey, F. A., & Prinz, M. (1978). Ultramafic inclusions from San Carlos, Arizona: Petrologic and geochemical data bearing on their petrogenesis. *Earth and Planetary Science Letters*, 38(1), 129–176. [https://doi.org/10.1016/0012-821X\(78\)90130-9](https://doi.org/10.1016/0012-821X(78)90130-9)
- Gibson, S. A., McMahon, S. C., Day, J. A., & Dawson, J. B. (2013). Highly refractory lithospheric mantle beneath the Tanzanian Craton: Evidence from Lashaine pre-metasomatic garnet-bearing peridotites. *Journal of Petrology*, 54(8), 1503–1546. <https://doi.org/10.1093/ptrology/egt020>
- Giuliani, A., Kamenetsky, V. S., Kendrick, M. A., Phillips, D., & Goemann, K. (2013). Nickel-rich metasomatism of the lithospheric mantle by pre-kimberlitic alkali-S-Cl-rich C-O-H fluids. *Contributions to Mineralogy and Petrology*, 165(1), 155–171. <https://doi.org/10.1007/s00410-012-0801-1>
- Giuliani, A., Phillips, D., Kamenetsky, V. S., Kendrick, M. A., Wyatt, B. A., Goemann, K., & Hutchinson, G. (2014). Petrogenesis of mantle polymict breccias: Insights into mantle processes coeval with kimberlite magmatism. *Journal of Petrology*, 55(4), 831–858. <https://doi.org/10.1093/ptrology/egu008>
- Giuliani, A., Phillips, D., Kamenetsky, V. S., & Goemann, K. (2016). Constraints on kimberlite ascent mechanisms revealed by phlogopite compositions in kimberlite and mantle xenoliths. *Lithos*, 240–243, 189–201. <https://doi.org/10.1016/j.lithos.2015.11.013>
- Griffin, W. L., Natapov, L. M., O'Reilly, S. Y., van Achterbergh, E., Cherenkova, A. F., & Cherenkov, V. G. (2005). The Kharantai kimberlite field, Siberia: Modification of the lithospheric mantle by the Siberian Trap event. *Lithos*, 81(1–4), 167–187. <https://doi.org/10.1016/j.lithos.2004.10.001>
- Hartmann, G. (1986). *Chemical composition and mineralogy of peridotite xenoliths with varying metasomatic overprint from basalts of the Hessian Depression*. PhD Thesis. Göttingen University.
- Hopp, J., Trierloff, M., Brey, G. P., Woodland, A. B., Simon, N. S. C., Wijbrans, J. R., et al. (2008). ⁴⁰Ar/³⁹Ar-ages of phlogopite in mantle xenoliths from South African kimberlites: Evidence for metasomatic mantle impregnation during the Kibaran orogenic cycle. *Lithos*, 106(3–4), 351–364. <https://doi.org/10.1016/j.lithos.2008.09.001>
- Ionov, D. A., Ashchepkov, I. V., Stosch, H.-G., Witt-Eickchen, G., & Seck, H. A. (1993). Garnet peridotite xenoliths from the Vitim Volcanic Field, Baikal Region: The nature of the garnet-spinel peridotite transition zone in the continental mantle. *Journal of Petrology*, 34(6), 1141–1175. <https://doi.org/10.1093/ptrology/34.6.1141>
- Kaesler, B., Kalt, A., & Pettke, T. (2006). Evolution of the lithospheric mantle beneath the Marsabit volcanic field (Northern Kenya): Constraints from textural, P-T and geochemical studies on xenoliths. *Journal of Petrology*, 47(11), 2149–2184. <https://doi.org/10.1093/ptrology/egl040>
- Kargin, A. V. (2021). Multistage mantle metasomatism during the generation of kimberlite melts: Evidence from mantle xenoliths and megacrysts of the Grib kimberlite, Arkhangelsk, Russia. *Petrology*, 29(3), 221–245. <https://doi.org/10.1134/S0869591121030024>
- Klügel, A. (1998). Reactions between mantle xenoliths and host magma beneath La Palma Canary Islands: Constraints on magma ascent rates and crustal reservoirs. *Contributions to Mineralogy and Petrology*, 131(2–3), 237–257. <https://doi.org/10.1007/s004100050391>
- Koornneef, J. M., Davies, G. R., Döpp, S. P., Vukmanovic, Z., Nikogosian, I. K., & Mason, P. R. D. (2009). Nature and timing of multiple metasomatic events in the sub-cratonic lithosphere beneath Labait, Tanzania. *Lithos*, 112S, 896–912. <https://doi.org/10.1016/j.lithos.2009.04.039>
- Larionova, Y. O., Sazonova, L. V., Lebedeva, N. M., Nosova, A. A., Tretyachenko, V. V., Travin, A. V., et al. (2016). Kimberlite age in the Arkhangelsk Province, Russia: Isotopic Geochronologic Rb-Sr and 40Ar/39Ar and mineralogical data on phlogopite. *Petrology*, 24(6), 562–593. <https://doi.org/10.1134/S0869591116040020>
- Larsen, J. G. (1982). Mantle-derived dunite and lherzolite nodules from Ubekendt Ejland, west Greenland Tertiary Province. *Mineralogical Magazine*, 46(340), 329–336. <https://doi.org/10.1180/minmag.1982.046.340.05>

- Lee, C.-T. A., & Rudnick, R. L. (1999). Compositionally stratified cratonic lithosphere: Petrology and geochemistry of peridotite xenoliths from the Labait Volcano, Tanzania. In *Proceedings of the 7th International Kimberlite Conference* (pp. 503–521).
- Litasov, K. D., Foley, S. F., & Litasov, Y. D. (2000). Magmatic modification and metasomatism of the subcontinental mantle beneath the Vitim Volcanic Field (East Siberia): Evidence from trace element data on pyroxenite and peridotite xenoliths from Miocene microbasalt. *Lithos*, 54(1–2), 83–114. [https://doi.org/10.1016/S0024-4937\(00\)00016-5](https://doi.org/10.1016/S0024-4937(00)00016-5)
- Marchev, P., Arai, S., Vaselli, O., Costa, F. G., Zanetti, A., & Downes, H. (2017). Metasomatic reaction phenomena from entrainment to surface cooling: Evidence from mantle peridotite xenoliths from Bulgaria. *Journal of Petrology*, 58(3), 599–640. <https://doi.org/10.1093/ptrology/egx028>
- O'Connor, T. K., Edgar, A. D., & Lloyd, F. E. (1996). Origin of glass in quaternary mantle xenoliths from Meerfeldermaar, West Eifel, Germany: Implications for enrichment in the lithospheric mantle. *The Canadian Mineralogist*, 34, 187–200.
- Qi, Q., Taylor, L. A., & Zhou, X. (1995). Petrology and geochemistry of mantle peridotite xenoliths from SE China. *Journal of Petrology*, 36(1), 55–79. <https://doi.org/10.1093/ptrology/36.1.55>
- Rosenbaum, J. M. (1993). Mantle phlogopite: A significant lead repository? *Chemical Geology*, 106(3–4), 475–483. [https://doi.org/10.1016/0009-2541\(93\)90046-L](https://doi.org/10.1016/0009-2541(93)90046-L)
- Sharygin, V. V., Golovin, A. V., Pokhilenko, N. P., & Kamenetsky, V. S. (2007). Djerfisherite in the Udachnaya-East Pipe kimberlites (Sakha-Yakutia, Russia): Paragenesis, composition and origin. *European Journal of Mineralogy*, 19(1), 51–63. <https://doi.org/10.1127/0935-1221/2007/0019-0051>
- Solov'Eva, L. V., Kalashnikova, T. V., Kostrovitsky, S. I., Ivanov, A. V., Matsuk, S. S., & Suvoro, L. F. (2017). Phlogopite and phlogopite-amphibole paragenesis in the lithospheric mantle of the Birekte Terrane (Siberian craton). *Doklady Earth Sciences*, 475(1), 822–827. <https://doi.org/10.1134/S1028334X17070273>
- Szabo, C., Vaselli, O., Vannucci, R., Bottazzi, P., Ottolini, L., Coradossi, N., & Kubovics, I. (1995). Ultramafic xenoliths from the little Hungarian Plain (Western Hungary)—A petrologic and geochemical study. *Acta Vulcanologica*, 7, 249–263.
- Tomanikova, L., Savov, I. P., Harvey, J., de Hoog, J. C. M., Churikova, T. G., Gordeychik, B. N., & Yagodinski, G. M. (2019). A limited role for metasomatized subarc mantle in the generation of boron isotope signatures of arc volcanic rocks. *Geology*, 47(6), 517–521. <https://doi.org/10.1130/G46092.1>
- Wang, J., Hattori, K., Jianping, L., & Stern, C. R. (2008). Oxidation state of Paleozoic subcontinental lithospheric mantle below the Pali Aike volcanic field in southernmost Patagonia. *Lithos*, 105(1–2), 98–110. <https://doi.org/10.1016/j.lithos.2008.02.009>
- Wartho, J.-A., & Kelley, S. P. (2003). $^{40}\text{Ar}/^{39}\text{Ar}$ ages in mantle xenolith phlogopites: Determining the ages of multiple lithospheric mantle events and diatreme ascent rates in southern Africa and Malaita, Solomon Islands (Vol. 220, pp. 231–248). Special Publications of the Geological Society of London. <https://doi.org/10.1144/GSL.SP.2003.220.01.14>
- Wulff-Pedersen, E., Neumann, E.-R., Vannucci, R., Bottazzi, P., & Ottolini, L. (1999). Silicic melts produced by reaction between peridotite and infiltrating basaltic melts: Ion probe data on glasses and minerals in veined xenoliths from La Palma, Canary Islands. *Contributions to Mineralogy and Petrology*, 137(1–2), 59–82. <https://doi.org/10.1007/s004100050582>